Climate engineering to mitigate the projected 21st-century terrestrial drying of the Americas:

A direct comparison of Carbon Capture and Sulfur Injection

Yangyang Xu[1, *], Lei Lin[2, *], Simone Tilmes[3], Katherine Dagon[3], Lili Xia[4], Chenrui Diao[1], Wei Cheng[5], Zhili Wang[6], Isla Simpson[3], Lorna Burnell[7]

[1]Department of Atmospheric Sciences, Texas A&M University, College Station, Texas 77843, USA
[2]School of Atmospheric Sciences and Guangdong Province Key Laboratory for Climate Change and Natural Disaster Studies, Sun Yat-Sen University, Zhuhai, Guangdong, 519000, China
[3]Climate and Global Dynamics Laboratory, National Center for Atmospheric Research, Boulder, CO, USA
[4]Department of Environmental Sciences, Rutgers University, New Brunswick, New Jersey, USA
[5]Mechanical and Aerospace Engineering, Cornell University, Ithaca, NY, USA
[6]State Key Laboratory of Severe Weather and Key Laboratory of Atmospheric Chemistry of CMA, Chinese Academy of Meteorological Sciences, Beijing, China
[7]University of Nottingham, UK

*_Correspondence to_ Yangyang Xu (yangyang.xu@tamu.edu) or Lei Lin (linlei3@sysu.edu.cn)

Abstract.

To mitigate the projected global warming in the 21st century, it is well recognized that society needs to cut CO2 emission and other short-lived warming agents aggressively. However, to stabilize the climate at a warming level closer to the present day, such as the "well below 2ºC" aspiration in the Paris agreement, a net-zero carbon emission by 2050 is still insufficient. The recent IPCC special report calls for a massive scheme to extract CO2 directly from the atmosphere, in addition to the decarbonization, to reach negative net emission at the mid-century mark. Another ambitious proposal is the solar radiation-based geoengineering schemes, including injecting sulfur gas into the stratosphere. Despite being in the public debate for years, these two leading geoengineering schemes have not been directly compared under a consistent analytical framework using global climate models.

Here we present the first explicit analysis of hydroclimate impacts of these two geoengineering approaches, using two recently available large-ensemble (>10 members) model experiments conducted by a family of state-of-art Earth system models. The CO2-based mitigation simulation is designed to include both emissions cut and carbon capture. The solar radiation-based mitigation simulation is designed to inject the sulfur gas strategically at specified altitudes and latitudes and run a feedback control algorithm, to avoid common problems previously identified such as the over-cooling of the Tropics and large-scale precipitation shifts.

Our analysis focuses on the projected aridity conditions over the Americas in the 21st century, in detailed terms of the potential mitigation benefits, the temporal evolution, the spatial distribution (within North and South America), the relative efficiency, and the physical mechanisms. We show that sulfur injection, in contrast to previous notions of leading to excessive terrestrial drying (in terms of precipitation reduction) while offsetting the global mean greenhouse gas (GHG) warming, will instead mitigate the projected drying tendency under RCP8.5. The surface energy balance change induced by Sulfur injection, in addition to the well-known response in temperature and precipitation, plays a crucial role in determining the overall terrestrial hydroclimate response. However, when normalized by the same amount of avoided global warming in these simulations, sulfur injection is less effective to curb the worsening trend of regional land aridity in the Americas under RCP8.5, when compared with carbon capture. Temporally, the climate benefit of Sulfur injection will emerge more quickly, even when both schemes are hypothetically started in the same year of 2020. Spatially, both schemes are effective in curbing the drying trend over North America. However, for South America, the Sulfur Injection scheme is particularly more effective for the sub-Amazon region (South Brazil), while the Carbon Capture scheme is more effective for the Amazon region. We conclude that despite the apparent limitations (such as inability to address ocean acidification) and potential side effects (such as changes to the ozone layer), innovative means of Sulfur Injection should continue to be explored as a potential low-cost option in the climate solution toolbox, complementing other mitigation approaches such as emissions cut and carbon capture (Cao et al., 2017). Our results demonstrate the urgent need for multi-model comparison studies and detailed regional assessment in other parts of the world.

1 Introduction

21st-century global warming, mostly driven by CO_2 emissions and other greenhouse gas emissions, is one of the greatest crisis facing the world today. A higher level of warming has been shown to lead to more frequent extreme weather and natural disasters (Schiermeier, 2011; Donat et al., 2013; Fischer and Knutti, 2015; Wang et al., 2017; Lin et al., 2018), all having profound implications for public health, agriculture and regional economy (Kunkel et al., 1999; Easterling et al., 2000; Knapp et al., 2008; Lesk et al., 2016). If left unchecked, temperature increases will soon pass the 1.5 and 2ºC warming levels (relative to the pre-industrial era) in the coming decades and continue to rise (Peters et al., 2012), calling for a stronger need to comprehensively assess the ecological and societal impacts at various warming levels and plan for adaptation at regional to local scales.

To mitigate the future accelerated climate change, the importance of cutting CO_2 emissions and a few short-lived climate pollutants (SLCPs) has been well recognized (Meinshausen et al., 2009; Shindell et al., 2012; Victor et al., 2015). But most recent analyses show that even with massive decarbonization to achieve a net-zero carbon emission by the mid-21st century, it is still not sufficient to stabilize global warming at a level relatively close to the present level (e.g., the 1.5ºC goal as proposed in the Paris agreement) (Xu and Ramanathan, 2017; Miller et al., 2017). Instead, aggressive climate engineering schemes are needed in order to meet these low-warming targets (Keller et al., 2014; Tilmes et al., 2016; Lawrence et al., 2018). Among the many creative approaches (e.g. spraying seawater over the sea ice (Leslie et al., 2018), ocean fertilization, marine cloud brightening, oceanic evaporation enhancement (Salter, 2002), and regional land albedo modification via vegetation or white roofs), two schemes that can have global impact have received the most considerable attention that leads to proof-of-concept technical design (Vaughan and Lenton, 2011). The first is carbon capture and storage that directly extracts CO_2 from the atmosphere, especially close to its emission sources where the ambient concentration is high (Herzog, 2001). The second is the sulfur injection into the stratosphere to reflect sunlight to space (Crutzen, 2006). Both approaches, especially the first one, can be expensive, and at the same time, could induce side effects, including those not yet identified. More scrutiny on the effectiveness and undesired consequences is thus urgently needed before any real-world deployment.

The utility of sulfur injection as a means to mitigate climate change has been long suggested (e.g., Crutzen 2006, Robock et al., 2009; Niemeier and Tilmes, 2017), but some potential drawbacks have also been identified (Pongratz et al., 2012; Keller et al., 2014; Effiong and Neitzel, 2016; Irvine et al., 2017). For example, a notable downside of sulfur injection (mostly designed to be initiated from the Tropics to offset the higher intensity of solar radiation there), is that it tends to over-cool the tropics while under-cooling the polar warming due to the amplified greenhouse gas effect (Moore et al., 2014). To address these shortcomings, the strategic design has been proposed (MacMartin et al., 2017) to inject sulfur gas at multiple latitudes and selected heights to keep the north-south and Pole-to-Tropics temperature gradient largely fixed, while lowering the global

mean temperature. By this design, global warming due to GHG will be balanced in a more spatially uniform fashion. Following the initial success of numerical tests in Kravitz et al., (2017), Tilmes et al. (2018, BAMS) conducted a large-ensemble model experiment (Geoengineering Largen Ensembles, GLENS) under the same rationale. A large-ensemble approach is particularly useful to assess climate impacts because extreme weather can be better quantified with a larger sampling, and the role of natural variability internal to the climate system can be more robustly isolated.

Utilizing this GLENS dataset, recent studies have looked at hydroclimate change under this Geoengineering method. Based on the analysis from Simpson et al. (2019), the precipitation in tropical and extratropical regions shows a dry-get-wetter, wet-get-drier pattern due to the aerosol induced stratospheric heating, opposite to the well-known pattern of dry-gets-driver response due to global warming. Cheng et al. (2019) also found the global land precipitation and evapotranspiration reduced slightly at the end of this century. Nevertheless, in both studies, the global soil moisture is well maintained by the geoengineering method except for India and the Amazon. Cheng et al. (2019) explained that the reduction of summer soil moisture in India and the Amazon is dominated by the decrease in precipitation.

Our study extends the scope of existing GLENS analysis, by placing the Sulfur Injection into the greater context of climate engineering (MacMartin et al., 2018, PTRS). Here we aim to compare the multiple metrics of mitigation "benefits" of Sulfur Injection with Carbon Capture, another more expensive and yet more fundamental approach (e.g., to mitigate ocean acidification). Because many other analyses using GLENS have documented the global impact of Sulfur Injection, here we choose to focus on a smaller region of North and South America, and on a specific set of land-based hydroclimate quantities that are of close relevance to agriculture, ecosystems, socioeconomics, and indirectly related to the terrestrial carbon cycle in the Amazon and its feedback to climate change.

The structure of the paper is the following. In Section 2, we provide the details of the model description, experiment setup, the observational dataset used as model calibration, and the rationale of deriving climate benefits. In Section 3, we present and compare the climate benefits of two geoengineering approaches on a global scale. The regional changes are presented in Section 4 with detailed discussions on the mechanisms of the distinct results over the sub-Amazon and Amazon regions. In Section 5, we discuss the results of climate responses in terms of normalized changes with respect to global temperature change. Section 6 further discusses the implications and makes concluding remarks.

2 Methods

2.1 Global Climate Models

Two fully coupled ocean and atmospheric models, which are identical for the ocean, and the tropospheric atmosphere component, are used in this study. The horizontal resolution of the atmosphere component for both models is set at 0.9º×1.25º.

CESM1-CAM5 (the Community Earth System Model version 1 with Community Atmosphere Model version 5, short as "CESM" after this) is a global climate model that consists of coupled atmosphere, land, land-ice, ocean, sea ice, the diagnostic biogeochemistry module component models, plus one coupler component. A new moist turbulence scheme explicitly simulates stratus-radiation-turbulence interactions, making it possible to simulate full aerosol indirect effects within stratus. A new shallow convection scheme uses a realistic plume dilution equation and closure that accurately simulates the spatial distribution of shallow convective activity. Computation of an updraft vertical velocity now allows for aerosol-cumulus interactions. The revised cloud macrophysics scheme provides a more transparent treatment of cloud processes and imposes full consistency between cloud fraction and cloud condensation. Stratiform microphysical processes are represented by a prognostic, two-moment formulation for cloud droplet and cloud ice, and liquid mass and number concentrations. The radiation scheme has been updated to the Rapid Radiative Transfer Method for GCMs (RRTMG) and employs an efficient and accurate correlated-k method for calculating radiative fluxes and heating rates. The 3-mode modal aerosol scheme (MAM3) has been implemented and provides internally mixed representations of number concentrations and mass for Aitkin, accumulation, and coarse aerosol modes.

Sharing most of the features described above, CESM1-WACCM (the Community Earth System Model version 1 with the Whole Atmosphere Community Climate Model, short as "WACCM" hereinafter) is a chemistry-climate model of the Earth's atmosphere, from the surface to the lower thermosphere. A finite-volume dynamical core (Lin, 2004) is used for the tracer advection. The vertical resolution ranges from 1 to 2 km over the lower stratosphere and the tropopause. The land model CLM4.5 has fixed distributions of vegetation including interactive carbon and nitrogen cycles. CLM4.5 allows leaf area indexes to respond to climate changes. The Ball-Berry stomatal conductance model was utilized. The stomatal conductance is directly influenced by the relative humidity at the leaf surface, the CO_2 concentration at the leaf surface, and the soil water.

The major difference between the WACCM and CESM models is the stratospheric atmosphere component. The WACCM has a high-top configuration that extends to about 140km ($6x10^{-6}$ hPa) and has a comprehensive representation of stratospheric chemical and dynamic processes (Mills et al., 2017), both crucial to simulate the radiative impact of stratospheric aerosols (via volcanic or artificial injection). The sulfur injection large ensemble simulation is only available in the WACCM version.

CESM has a typical model top at around 40 km, and the CO2 mitigation large ensemble simulation is only available in this model version.

Note that the model structural differences here can affect simulated climate response. The climate sensitivity is 4.1 K under doubling of CO2 for CESM and 5.2 K for WACCM (similar to a new version recently released; Gettleman et al., 2019). Both are within the CMIP5 range and are more in line with the higher CMIP6 range. Additionally, The land components are also different between these two versions due to incremental model development. CESM used an earlier version of CLM4 and WACCM used an updated version of CLM4.5. According to Cheng et al., (2019), relative to the earlier version CLM4, CLM4.5 includes modifications of hydraulic properties of frozen soils and thus some seasonal changes in Arctic temperature. In the following analysis, we made attempts to address the caveat of model differences by (a) applying corresponding bias corrections to future climate response simulated by these two models, separately (Section 2.5), and (b) normalizing the response with respect to the temperature response (Section 5).

2.2 Numerical Experiments

Two pairs of model simulations were conducted and published in the last few years, both featuring a large ensemble to enhance the robustness of examined climate responses, especially at a regional level. The WACCM set (http://www.cesm.ucar.edu/projects/community-projects/GLENS/) is aimed at stabilizing the climate at its 2020 level with sulfur injection. The CESM set (low warming large ensemble, http://www.cesm.ucar.edu/experiments/1.5-2.0-targets.html) is aimed at climate stabilization at 1.5 and 2ºC warming levels, with aggressive emission cut and rapid growth of negative emission technology, an extreme mitigation scenario. Land cover and land use in these two pairs of simulations are consistently the same as in RCP8.5.

With the two sets of paired simulations, the effect of the two geoengineering approaches can be assessed by contrasting the run with geoengineering applied with the baseline potential warming worlds, which we would refer to as the climate “benefits". Of course, for specific regions and certain climate variables, it may turn out that the climate “benefits" are negligible or even negative – i.e., geoengineering makes climate change under RCP8.5 even worse.

a. Stratospheric Sulfur Injection

The simulations were conducted with WACCM: one with baseline emissions (RCP8.5) and the other with Sulfur injection applied at 2020 and afterward (hereafter referred to as “Sulfur Injection”). The amount and location of Sulfur Injection were strategically selected to stabilize the temperature at the present-day level and minimize the undesired perturbation to the

latitudinal temperature gradient (Tilmes et al., 2018). The simulation was repeated multiple times (see Table 1 for details) to form a larger ensemble (Geoengineering Large ENSemble, GLENS, Tilmes et al., 2018), which enhances the statistical significance of the assessed climate impact, especially at a regional level.

b. Carbon Capture

Similarly, two simulations were conducted with CESM: one with baseline emissions (RCP8.5) and the other with CO_2 removal and emissions cuts applied to start in 2015-2020 (hereafter referred to simply as "Carbon Capture"). This scenario is constructed to be a much more aggressive decarbonization pathway than RCP2.6 (see details in Sanderson et al., 2017). Net-zero carbon emission is thus reached at 2050, beyond which the net emission turns negative, which helps the planet to stabilize at 1.5ºC warming level, just slightly higher than the present-day (2010-2019) temperature level. We show the mass amount of CO_2 reduced (combining emission cut and various ways of net emission technology) and the associated negative radiative forcing in Figure 4 to illustrate the idealized trajectories and to compare with well-studied RCP2.6. However, the technical feasibility and required socio-economic shift to facilitate the scale-up of capacities such as direct air capture (Hanna et al., 2020) and clean energy transition (Hanna et al., 2020b) are beyond the discussion of this paper.

2.4 Hydroclimate variables examined

In this study, we focus on climate quantities over land due to their close relevance to agriculture, ecosystems, and the carbon cycle, which include:

a. T: surface air temperature at the reference height of 2 m above the ground.
b. P: total precipitation, which includes rainfall and snowfall without differentiating large-scale or convective components as formulated in the model.
c. PET: potential evapotranspiration, which represents the atmospheric demand for water. PET is calculated using model output, following the physically based Penman-Monteith equation (Shuttleworth, 1993), which includes key parameters of surface air temperature, surface available energy, surface wind speed, and relative humidity.
d. Aridity Index (P/PET).
   The aridity index is calculated as the simple ratio of annual P and annual PET (Mortimore et al., 2009; Hulme, 1996; Middleton and Thomas, 1992). P/PET is highly correlated with vegetation types (Feng and Fu, 2013; Huang et al., 2017). Using the P/PET classification by the United Nations Convention to Combat Desertification (United Nations Convention to Combat Desertification, 1994), drylands (characterized by P/PET <0.65) further classify various types,

including sub-humid (0.5< P/PET <0.65), semi-arid (0.2< P/PET <0.5), arid (0.05< P/PET <0.2), hyper-arid (P/PET <0.05).

e. Other variables to depict aridity and corroborate Aridity Index.

To further test the utility of P/PET as a metric to depict aridity conditions, we show the similar temporal evolution of P/PET with soil moisture, and that between PET and actual ET (another metric commonly used) over major land regions (60ºS to 60ºN) in Figure 1. Spatial patterns also show similar agreement between P/PET and soil moisture as well as P-ET (another metric commonly used) for both present-day and future change (Figure 2), again supporting the appropriateness of using P/PET as an aridity metric.

2.5 Bias correction of the raw model results

Climate model output cannot be taken at its face value, especially for future projection. The analysis, especially regarding the future projection, must consider the potential model bias in simulating the past and the present as well as the uncertainty inherent to climate models that are so far poorly constrained. Considering these, we corrected the model simulated T, P, and PET based on the observational dataset, following the approaches in Dai (2011) and Feng and Fu (2013). The NOAA Climate Prediction Center (CPC) data (Fan and van den Dool, 2008; Chen et al., 2002) is used as the benchmarking temperature and precipitation over land. The Global Land Data Assimilation System (GLDAS) (Todell et al., 2004) provides the surface sensible heat flux and latent sensible heat flux, specific humidity, and wind speed to derive the observation-based PET as in Feng and Fu (2013). The climate variables over the ocean are not corrected and thus not analyzed in this study.

The bias correction based on the observational dataset is only directly applied to CESM_Historical (with 30 runs from 1975 to 2005). The bias correction will force the model output to agree with the observed 1975-2005 climatology (and remove the bias of the seasonal cycle if any), but not necessarily agree with the observation every year. In a nutshell, the temperature is adjusted using the addition/subtraction of identified biases on a monthly basis. For P or PET, the variables are adjusted using multiplication/division of identified biases on a monthly basis. A multiplication/division is used instead of addition/subtraction to avoid the negative numbers for P or PET. Note that the difference between WACCM_RCP8.5 and WACCM_SulfurInjection will yield the "impact" of sulfate injection. The impact will change compared to raw data without bias correction because, for precipitation and PET, the bias correction is done via multiplication/division, not simple addition/subtraction.

The same bias correction is applied to future simulations of CESM (CESM_RCP8.5 and CESM_CarbonCapture, in 2006 and afterward), which branched from the CESM_Historical in 2005. For WACCM_RCP8.5 simulations, we indirectly adjust them to agree with the corrected CESM_RCP8.5 in 2010-2019 ("present-day"). We could not adjust WACCM directly based on

observations because the WACCM-RCP8.5 simulation only starts in 2010 and overlaps with the observation record (ending in 2019) for less than ten years. Similarly, WACCM_SulfurInjection was adjusted to match with WACCM_RCP8.5 in 2020 (when it branches from WACCM_RCP8.5).

3 Global mitigation

3.1 Temperature

In Figure 3, we show the long-term changes simulated by all four model experiments (two baseline worlds and two mitigated climates via different geoengineering schemes). We focus on the following three periods: present-day (2010-2019), mid-century (2046-2055), and end-of-century (2086-2095). Without the bias correction, the models do not agree on T and P for the recent period of 2005-2020 (Figure 3 a-b; and also see the regional map in Figure 2, the first row). Therefore, it is essential to apply the bias correction to model output before carrying out a meaningful comparison of future changes. For example, comparing Fig 3b and d, WACCM appears to have a 25% positive bias for precipitation over major land, and CESM has a smaller positive bias.

Comparing the bias-corrected model output (Figure 3, c and d), because of the larger climate sensitivity, WACCM warms up faster than CESM, reaching a 6ºC warming over land under RCP8.5 just within this century (T (2086-2095) - T(2010-2019), which is ~7ºC relative to pre-industrial, thus posing an existential threat to mankind if it comes true (Xu and Ramanathan, 2017). The CESM with a climate sensitivity of 4ºC simulates a 4.7ºC warming over the major land areas during the 21st century. The two types of mitigation efforts, by design, would lead to a similar amount of temperature stabilization to a level close to the present-day. The Sulfur Injection simulation here leads to a cooling of 6ºC towards the end of the century, compared with the baseline warming. This larger cooling is designed to largely balance the projected warming by introducing a large amount of sulfur gas, some from locations off the tropics (Tilmes et al., 2017; and Kravitz et al., 2018).

The mid-century warming over global major land projected by those two models amounts to 2.0 to 2.5ºC compared to the present-day (Table 2). Sulfur Injection can completely offset the warming by 2.4ºC, while Carbon Capture can only mask about 70% of 2.0ºC by 1.3ºC. Even though the carbon capture scheme is introduced slightly earlier in 2015 to 2020, the longer lifetime of CO2 makes the impact of perturbation to the carbon cycle and atmospheric concentration slower to emerge (Figure 4e vs. f), compared to Sulfur Injection. This additional inertia (or lag) in CO2 emission-based mitigation is well noted when the CO2 emission cut was previously contrasted with the mitigation of short-lived climate pollutants (e.g., Hu et al., 2013). Towards the end of the century, the lagging effects in the Carbon Capture case become negligible, and both schemes can

almost completely offset the projected warming in the baseline by 4.0ºC and 5.7ºC, out of the 4.5ºC and 5.8ºC baseline warming, respectively (Table 2, Column 1 right).

3.2 Precipitation

Similar lagging effects are also found for global land precipitation. Table 2 shows that the mid-century reduction due to Carbon Capture is 31% of the projected increase (23.0 mm/year), and the Sulfur Injection can reduce the precipitation increase by as large as 75%. Again, towards the end of the century, the difference between the two cases, in terms of potential mitigation benefits, becomes smaller (62% reduction by Carbon Capture and 98% by Sulfur Injection).

The close to 100% reduction of precipitation increase due to Sulfur Injection is worth commenting on. Because of the lack of direct radiative heating in the troposphere, such as due to CO_2 or black carbon aerosols, sulfate aerosols will have a larger precipitation effect (per degree of global mean temperature change) compared to CO_2 (Lin et al., 2016; 2018). Another alternative perspective to explain the over-drying (or the slowdown of the hydrological cycle) due to geoengineering is the increase in atmospheric stability and suppressed evapotranspiration, especially in the tropics which tends to be over-cooled in previous Sulfur Injection model experiments. As a result, when the amount of Sulfur Injection is carefully adjusted to balance the CO_2 warming, total rainfall will usually be excessively suppressed (so-called "over-drying") (e.g., Bala et al., 2008; Jone et al., 2013; Tilmes et al., 2013; Crook et al., 2015).

However, in this WACCM setup, the over-drying consequence, especially over the tropics, is dampened. This is likely due to the following reason. In the current experiment design, Sulfur Injection is more greatly introduced to the extratropical region, and thus induces a much-reduced tropical overcooling compared to previous stratospheric geoengineering experiments. Indeed, the global mean temperature, as well as the north-south gradient, will be well preserved while offsetting the baseline CO_2 warming. This relatively weaker tropical cooling (again, because of the larger forcing imposed off the tropics) leads to a smaller over-drying in terms of precipitation, despite a persistent suppression of large convective precipitation (Simpson et al. 2019). From Figure 3d, Sulfur Injection will lead a negligible decrease in precipitation by 4-6 mm/year (WACCM_SulfurInjection: 2086-2095 vs. 2020-2029), over the majority of the land. The over-drying is stronger (12-15 mm/year) if the model output is not bias adjusted (Figure 3b). This over-drying, despite being small in this model, is considered as a side effect of Sulfur Injection and often used as an argument against its deployment. In contrast, the Carbon Capture falls short in offsetting the full magnitude of projected precipitation increases (green line in Figure 3b, d), and thus will not run into the problem of "over-drying".

The applicability of this precipitation-centered perspective in assessing terrestrial aridity will be put into the test in the next subsection.

3.3 PET and P/PET

It is increasingly well-recognized that precipitation alone does not reflect the full effects of the hydrological cycle on the terrestrial ecosystem. A full suite of aridity indices has been developed and is continuously being improved to provide a better depiction of aridity conditions (Mishra and Singh, 2010). It is beyond the scope of this paper, which emphasizes the contrast of two climate engineering schemes, to discuss the advantages and limitations of those approaches. However, we included more than one indicator from the model output to examine the robustness of our results largely based on P/PET. We showed that ET and soil moisture are closely correlated with PET and P/PET, respectively, over the global scale (Figure 1). Moreover, Figure 2 shows that a broad agreement between P/PET, soil moisture, and P-ET exists not only for the present-day climatology but also for the future increase under the warming scenarios.

The major difference between the two geoengineering approaches, when viewed on a global scale, is due to PET. Despite an increase in P, the projected PET growth that approximately scaled with T increase will exacerbate future land aridity (Fu and Feng, 2014; Scheff and Frierson, 2014). Indeed, the projected P/PET under RCP8.5 (Figure 3f) is decreasing over the major land in both sets of model simulations, with a larger magnitude in CESM than WACCM (also seen in the last two columns of Table 2). The two geoengineering schemes can both limit PET growth (Figure 3e) to reduce the tendency of worsening aridity, but with considerably large differences in the magnitude and timing, as detailed below.

On the magnitude. The Carbon Capture can lower the projected increase in PET by 60% to 83% at the mid-century and end of the century, respectively, which leads to an almost complete offset of P/PET decline (see green line of Figure 3f). Therefore, the mid-century and end-of-century P/PET are mostly the same as the present-day value, except for the near-term (prior to 2040) drop in P/PET due to the lagging effects of CO_2 mitigation which will be elaborated later (Figure 4). On the other hand, Sulfur Injection leads to a major decrease in PET that flips the sign of the projected increase due to GHG warming (Figure 3e). For example, the mid-century projected PET increase is 102.2 mm/year, but the Sulfur Injection can reduce that by 127.8 mm/year, which actually leads to a drop of the absolute value of PET by 25.6 mm/year. The larger reduction in PET due to Sulfur Injection also reflects in the larger increase in P/PET by 0.03 to 0.05, despite a smaller projected P/PET decline in the baseline WACCM warming.

The large response of P/PET due to Sulfur Injection to more than offset the baseline changes can be clearly seen in Figure 3f (blue line). Different from all other curves, Sulfur Injection mitigated P/PET features an increase in absolute value, making

the geoengineered climate over land overall "wetter" than the present-day, despite a reduction in precipitation. Although both types of geoengineering can stabilize temperature at a level close to present-day, Sulfur Injection appears to have this additional "benefit" of flipping the sign of the drying trend as projected in the baseline scenarios.

On the timing. The increase in P/PET due to Sulfur Injection is mostly achieved in the near term (before 2050), due to the quick response time. Figure 4 b-d shows the mitigation effects (the difference between the paired simulations) in percentage relative to present-day, which highlights the response due to two approaches in the near-term and long-term. During the first 30 years of the deployment (2020-2050), Sulfur Injection leads to a quick reduction of PET of 2.8 %/decades than the decrease of P at 1.2 %/decades, and thus causes the P/PET to increase (note the Y-axis for Figure 4d is flipped to aid visual comparison). After 2050, when the precipitation decreases at a greater rate of 0.9 %/decades, the P/PET increase in response to Sulfur Injection will slow down (with the rate dropping by more than half from 1.5 %/decade to 0.7 %/decades). This non-monotonic behavior in Sulfur Injection induced a P/PET response that is highly distinct from the Carbon Capture case in terms of timing. The latter, in contrast, always falls behind the Sulfur Injection changes in inducing climate responses (green vs. blue in Figure 4a-d). The P/PET enhancement due to Carbon Capture (compared to baseline warming, not to present-day), only starts to be significant toward the end of the century with a growth rate of 1.4%/decades after 2050, almost three times larger than the decades before 2050.

3.4 Summary: faster/stronger benefits due to Sulfur Injection

In terms of mitigation at a global scale, we emphasize P/PET is closely tied to land aridity conditions and vegetation response (Huang et al., 2017), rather than P itself. Note that we select P/PET among other drought indicators to avoid the complexity of the analysis because the main goal of our analysis is to compare highly extreme mitigation scenarios. Fig 2 revealed regional discrepancies that suggest for a more comprehensive drought assessment, more metrics should be included in addition to P/PET.

Our results here suggest that Sulfur Injection not only offsets the projected worsening in aridity in the 21st century but also, surprisingly, leads to recovery from the present-day condition, which is already worse than pre-industrial conditions or even just decades ago. More encouraging, the recovery ("wetting" over major global land) is detectable in the near term (MacMartin et al. 2019). Carbon Capture, in contrast, has a weaker (even in relative terms) and slower mitigation benefit and does not lead to the full reversal of P/PET as in response to Sulfur Injection. The response time of these two approaches is illustrated in Figure 4e and f. Although the CO2 amount reduced (Figure 4e) has a quick increase after the deployment (2020), the radiative forcing due to the reduced CO2 concentration (Figure 4f) takes a slower trajectory to increase and is always falling behind the negative forcing due to Sulfur injection.

The quicker and stronger response to Sulfur Injection, suggests a benefit from the deployment, providing a further incentive for adopting this scheme. However, because of the quicker response, one could counter-argue that Sulfur Injection should be reserved as the "last resort" option only used when the CO2 warming becomes too large towards the end of the century.

4 Regional responses in the Americas

How do the results and arguments above hold over specific regions? Next, we present a detailed comparison over North America, and South America and discuss the mechanism. Other recent works have studied the precipitation response in various regions. Cheng et al., (2019), using soil moisture as the metric, have found major regions that would benefit from the Sulfur Injection in having the aridity trend reverted. However, certain regions will have aridity conditions worsened in the Sulfur Injection scenario. Here we focus on North and South America using both P and P/PET to depict the full picture of hydrological response.

4.1 North America

The main reason for focusing on North America is the arid land expansion from American West into the Great Plains. The so-called 100th meridian, which traditionally separates the dry and mild climate, will likely shift eastward in future climate (Seager et al., 2018). This is clearly shown in the projection of both models with a major decrease in P/PET over the Great Plain regions by 10% to 20% (Figures 5 and 6). The corresponding change in absolute terms of P/PET is shown in Figure 2. The slight increase (light blue) over the intermountain western US regions does not pass the significance test in being different from the baseline simulations.

For North America, it is clear that the Sulfur Injection has a stronger effect than Carbon Capture, especially for the Central US in the mid-century (Figure 5 vs. Figure 6). Towards the end of the century, the Sulfur Injection increases P/PET by 0.05 (7.2%), while the Carbon Capture can eliminate the projected decrease in P/PET (Figures 5 and 6). This is largely consistent with the results of Eastern US (although to a lesser extent for the latter) and the responses over global major land (Figure 6, also illustrated in the time series of Figure 3).

The large decrease in PET in response to Sulfur Injection is the main reason for a slight increase in P/PET compared to present-day conditions in the geoengineered cases. The P/PET changes over the US are consistent with the tendency of the global major land (Figure 6d), and also largely supported by other metrics (soil water and P-ET in Figure 6 e,f).

Another way to examine the severity of aridity evolution is by further classifying the dryland into a few sub-types. These subtypes are classified by P/PET values, which are shown in the color bars in Figure 5 first row). The global arid area (P/PET ranges of 0.2 to 0.5) would increase from 15 million km2 in the historical period to 16.6 million km2 under the warming at the end of the century. The Carbon Capture can reduce it to 15.1 million km2, but Sulfur Injection can more than offset it to lower it to 13.5 million km2. Over North America, the results are generally similar, with a stronger reversal over the semi-arid area (P/PET ranges of 0.5 to 0.65) due to Sulfur Injection than Carbon Capture.

4.2 South America

The main reason for focusing on South America is the drying over the Amazon (by more than 30% using P/PET as the metric) could lead to die out of the rainforest and decrease the carbon sink and cause an increase in forest fires – major positive feedback that's missing in most of the global model projections so far, including the ones presented here.

While the changes over North America are largely consistent with global land change, South America's responses are more complicated. Notably, there is a major difference between northern Brazil, where the Amazon rainforest is mostly located, and the southern part of the nation (green and purple boxes in Figure 5a).

Northern Brazil will see a major decline of P/PET of 0.2 to 0.4 (15 to 30% relative to present-day) in the baseline warming cases (Figure 5), the largest among the four regions we considered in this study, transitioning the wetland into semi-arid dryland. This large decline of P/PET is a result of both PET increase as in other regions, but also P decrease that is unique in this tropical land, in contrast to other regions examined. If the RCP8.5 projection turns out to be true for the 21st century, a major consequence is the fate of the rainforest and its carbon uptake capacity. Given the high stakes, a relevant question is whether the two geoengineering schemes are able to revert the drying trend over the Amazon.

The CESM results show that Carbon Capture can essentially overturn the baseline drying and keep the P/PET at the same level as the present-day (Figure 5). This is achieved by both offsetting the precipitation decrease, but more importantly, by offsetting the projected PET increase by 80 to 90 % (Figure 7 b,c). The Carbon Capture (green in Figure 7b) mitigated climate will lead to a small increase in precipitation (relative to present-day) in northern Brazil, associated with a much smaller regional warming (<0.5ºC) than baseline (4.5ºC) (Figure 5). Note that the regional precipitation change can be hard to project at the sub-continental scale, and thus, the CESM simulated Carbon Capture response could be model dependent.

On the other hand, the WACCM results show that Sulfur Injection falls short of completely overturning the drying tendency over Northern Brazil in the baseline warming but can mitigate the drying magnitude by 60% by the end of the century. The

reason for the insufficiency of Sulfur Injection is that, despite a substantial reduction in PET (Figure 7c, going from 0.8 to 0), the WACCM results continue to produce a stronger precipitation reduction (relative to present-day) in the case of Sulfur Injection (blue dots in Figure 7b), unable to revert the precipitation reduction in the warming baseline. This additional suppression of tropical rainfall due to Sulfur Injection is also previously reported in Simpson et al., (2019), which concluded that the dynamical response to stratospheric heating played an important role during the JJA (but not in the DJF).

Although the simultaneous reduction of PET in response to Sulfur Injection leads to the end results of "wetting" (in terms of P/PET increase (brown and blue points in Figure 7d), the magnitude (roughly a 50% offset) is small compared that due to Carbon Capture (an offset by almost 100%, green and red dots in Figure 7d), in which the precipitation is flipped in sign to increase slightly, rather than just with the baseline decrease mitigated (green in North Brazil, Figure 7b). Overall, there is a weaker mitigation of the P/PET drying trend in response to Sulfur Injection compared to Carbon Capture over Northern Brazil. However, interestingly, the opposite is true for the sub-Amazon region, which is detailed below.

Unlike Sulfate Injection, Carbon Capture is consistently capable of mitigating the projected drying trend almost entirely over South America (similar to the global and eastern US cases). Despite being smaller than the Sulfur injection, there is sufficient capacity of Carbon Capture in overturning the drying trend over the sub-Amazon (from a 0.08 reduction of P/PET to almost zero), again due to a large reduction in PET, despite slightly weakened precipitation. This suggests again that focusing on P alone may lead to a biased interpretation of the projected and mitigated trends. Notably, Sulfur Injection induces a much larger increase in P/PET ("wetting") over the sub-Amazon, compared to Carbon Capture, actually offsetting the projected P/PET decrease by 150%. This is due to a regional increase in precipitation, which adds on top of PET reduction, to cause a larger increase of P/PET. The mechanism is exactly the flip side of Sulfur Injection's smaller capacity (by only 60%) to revert P/PET decline over the Amazon (Northern Brazil), where the precipitation is projected to further decrease in response to Sulfur Injection, despite a strong local cooling effect.

Synthesizing the precipitation changes over the Amazon (Northern Brazil) and sub-Amazon (Southern Brazil), the precipitation (especially in the JJA season as in Figure 5 of Cheng et al., 2019) is shifted from the deep tropics to the subtropics in response to Sulfur Injection, leading to an actual increase in precipitation over the sub-Amazon by 36.5 mm/year, rather than just offsetting the 18.2 mm/year decrease in the baseline warming case.

A substantial reduction in PET over sub-Amazon (but consistently true for other sub-regions explored in Figure 7), working together with the precipitation increase, would induce a large increase in P/PET (0.2) relative to the baseline case, more than enough to offset the projected decrease of 0.15 and actually to lead to P/PET increase by 0.05. Considering that this region at

the present-day is already subject to a detectable drying, such an over-compensation in P/PET in response to Sulfur Injection should be viewed as beneficial to the regional climate and ecosystem, a point we have stressed for the global mitigation results, but want to echo again here for sub-Amazon regions.

4.3 Summary: the unique responses over Amazon (North Brazil)

Overall, over three out of four regions examined here (Western US, Eastern US, and Southern Brazil, except for Northern Brazil), Sulfur Injection has a larger capacity in not only mitigating but also flipping the projected drying tendency. This is evidenced by the large response seen in the spatial maps of Figure 6 (especially the larger response in the mid-century due to time lag effects discussed in Section 3.1). A complete reversal to even increase in P/PET drying highlights the benefit of Sulfur Injection, at least for these three regions. On the other hand, Carbon Capture can almost completely offset the P/PET change by 100%, also the desired outcome. The mechanisms to achieve this complete offset can vary from one region to another, sensitive to the regional precipitation projection in the baseline and mitigated scenarios (e.g., over the western US), and thus potentially sensitive to model configurations. The responses over these three regions are found to be generally representative of the global mean (e.g., Figure 7 "major land" results with smaller error bars), which are presumably less subject to model diversity issues.

The South America regions present a clear argument that a precipitation-centered viewpoint may mistakenly overestimate the Sulfur Injection side effect in causing aridity by ignoring its accompanying suppression on PET. The contrasting results of Sulfur Injection to overcome the global drying tendency, when using precipitation only or using P/PET, is clearly demonstrated for the Amazon region, but also similarly true for other regions such as the Eastern US (to a lesser extent). For example, in Figure 6, the precipitation change over the Eastern US is slightly negative compared to present-day (“over-drying”) but become slightly positive in P/PET, suggesting an actual “wetting”, which is an improvement from the drying condition already detectable at the present-day (2010-2019) compared to the pre-industrial era.

One exception to the summary above is Northern Brazil (Amazon region). The Sulfur Injection, but not Carbon Capture, can only partially offset the projected drying, due to a further decrease in precipitation locally in the deep tropics (Figure 8b), which features a rainfall shift from the deep topics to subtropics (Figure 6). In response to Sulfur Injection, there is a smaller amount of PET reduction from the baseline increase (Figure 7c), compared to the other three regions and global mean, presumably due to extensive cloud cover over the tropical land, but could also be due to the vegetation difference between Northern Brazil and Southern Brazil.

5 Normalized changes with respect to global temperature change

The absolute value of climate benefits (including those presented in Table 2 and Figure 7) is dependent on the strength of geoengineering measures and thus can be less useful in a broader context. What is more informative is the physical mechanism governing the changes. In order to elucidate the different mechanisms contributing to the simulated changes over North and South America, we next examine the individual climate variable's contribution to P/PET changes, in a normalized (%/ºC) perspective.

In the following analysis, we show that even though Sulfur Injection has led to a larger mitigation benefit as detailed in the previous sections, it is mainly due to the larger forcing introduced and the larger global cooling realized (close to 6ºC). Sulfur Injection is less effective in mitigating the aridity worsening when the mitigation is normalized by the global cooling realized.

Figure 8 shows that the normalized changes have largely the same spatial pattern as in the absolute values presented in Figure 5, but the Sulfur Injection induced changes are now of similar magnitude compared to the Carbon Capture case for both time periods, with a slightly larger value for the mid-century but smaller values at the end of the century. Note that because of the normalization, some of the Amazon and sub-Amazon regions have changes less than 1 %/ºC (white area in Figure 8), in response to Carbon Capture and Sulfur Injection, suggesting an insignificant change of aridity condition if the global mean temperature mitigation is smaller than 1ºC. The Great Plain of the US, however, would benefit from either of the two geoengineering schemes, with a change as large as 5%/ºC to 10%/ºC.

What explains the weaker normalized P/PET response of Sulfur Injection? The relationship of various quantities (P, PET, P/PET) with respect to global mean temperature changes is further illustrated in the scatter plots (Figure 9), with the slope representing the sensitivity of P, PET, P/PET to global cooling induced by the two geoengineering schemes (4 to 6ºC of cooling in the x-axis). The calculated slope using the "linear fit" in Figure 9 is summarized in Table 4 and compared with another method of deriving the sensitivity, using the epoch difference between the two end-of-century contrasting "epochs". Note we have also tested the robustness of the linear regression approach by using decadal mean (also shown in Table 4) or annual mean (as in Figure 9), which turns out to yield a small difference. For example, the precipitation sensitivity changes from 2.6 %/ºC (Figure 9a) to 2.7 %/ºC at a global scale (Table 4).

The larger sensitivity in precipitation due to sulfur injection (Figure 9) is well understood (Muri et al., 2019; Niemeier et al., 2013), as a distinct feature of fast adjustment to stratospheric aerosol forcing (and also solar forcing as indicated in many previous studies, such as Bala et al., 2009; Duan et al., 2018). The large sensitivity to aerosols is also largely consistent with previous results contrasting tropospheric SO2 and CO2 increase (e.g., Ming et al., 2007; Wang et al., 2017). The larger slope of precipitation due to Sulfur Injection in WACCM is consistent with our previous study (Lin et al., 2016), but the magnitude

of the response is smaller than that reported in a different model (CESM1) forced by the 20th-century tropospheric aerosol changes (Table 4, 6.7 %/ºC). In contrast, Carbon Capture induced precipitation response (1.1 %/ºC) is of similar magnitude when compared with the 20th century CO2 increase examined with the same model (CESM1 in Lin et al., 2016; 1.2 %/ºC).

Different from the precipitation sensitivity, the PET sensitivity to Carbon Capture and Sulfur Injection are similar (3.8 %/ºC vs. 4 %/ºC). A similar PET change, when combined with the greater precipitation decrease, will lead to a smaller increase in P/PET in response to Sulfur Injection. In other words, the almost identical PET sensitivity in response to Sulfur Injection and Carbon Capture is the main reason that Sulfur Injection has a smaller control over P/PET by a factor of two (Figure 9, -1.1 %/ºC vs. -2.2 %/ºC). If Sulfur Injection leads to a greater amount of surface radiation reduction in other models such as CESM1 as in Lin et al., (2016), the P/PET sensitivity due to Sulfur Injection could be as large as the Carbon Capture case here. For example, Lin et al., 2016a previously found that the tropospheric SO_2 will lead to a much stronger PET sensitivity (6.3 %/ºC) than CO_2 (4.6 %/ºC) because of the surface solar radiation reduction. In this study, the PET response to Sulfur Injection (4 %/ºC) is only slightly higher than that due to Carbon Capture (3.5-3.8 %/ºC depending on the method of normalization).

Another complexity arises. Our previous 20th century-based analysis (Lin et al., 2016a) shows that tropospheric sulfate-induced PET changes strongly by 6.3 %/ºC. However, it still falls short of compensating the large precipitation decrease by 6.7 %/ºC, thus producing a small decline of P/PET (by only 0.4 %/ºC) in response to tropospheric sulfate cooling, opposite to the larger increase of P/PET in response to stratospheric Sulfur Injection (-1.5 %/ºC). The current model experiment precludes a definite answer to understanding the discrepancy of Sulfur induced P, PET, and P/PET responses, because of model difference (WACCM here vs. CESM in Lin et al., 2016a) and forcing difference (stratospheric here vs. tropospheric in Lin et al., 2016a). We speculate that the difference is mainly from the forcing difference because the stratospheric aerosols can be less effective in changing surface energy balance than tropospheric aerosols, which can induce warm cloud changes and are more concentrated over the land.

The speculation above is worth testing, for example, using the volcanic forcing experiment in the Last Millennium Ensemble (LME, using CESM but with 2º resolution; Fu et al., 2017). Our analysis in Table 4 supports this argument. The GHG-only and aerosol-only results from LME are similar to Lin et al., 2016's results of CO2- and SO4-induced responses using the same model (but with 1º resolution). The volcanic eruptions (active during the three periods of 1250-1270/ 1450-1460/ 1800-1820) before 1850 induced much weaker P response (2.5 to 4 %/ºC) than tropospheric SO2, similar to the Sulfur Injection results reported here (but using the different model of WACCM). Also, what's similar to the Sulfur Injection results here, despite the model difference, is the overall increase in P/PET when stratospheric aerosol cooling is imposed (i.e., negative sensitivity of

P/PET in Table 4), suggesting the "benefit" of flipping the projected P/PET decrease via stratospheric Sulfur Injection could be robust and model-independent.

In Table 5, we further break down the induced PET and P/PET changes (%/ºC) into four key quantities that contribute to PET calculation. The surface wind and relative humidity are, in general, smaller contributors compared with T and surface energy, except that at the regional level. RH can increase in response to cooling and thus reduces the PET. The stronger surface energy perturbation due to Sulfur Injection compared to Carbon Capture, mainly due to the strong suppression of incoming solar radiation reaching the ground, is clearly a major contributor to the larger reduction of PET at a global level, but not so for South America (Figure 10), presumably due to the extensive background cloud covers. Similarly, the changes in P over South America are complicated (Figure 10), featuring a decrease of North Brazil rainfall given the Sulfur Injection cooling (0.9 %/ºC) but an increase in response to the Carbon Capture cooling.

To summarize, the weaker sensitivity of P/PET in response to Sulfur Injection globally, and the weaker response in absolute values over the Amazon region as shown in Section 4, are the two major counterarguments against the effectiveness of Sulfur Injection. The comparison with our earlier studies on tropospheric SO2 and volcanic eruption using different model configurations (the 20th century or Last Millennium; CESM with 1º or 2º resolution) demonstrate qualitative robustness of the results and the common physical mechanisms.

6 Concluding Remarks

By examining the response of land hydroclimate to two types of geoengineering approaches, we show that Sulfur Injection will lead to land wetting when the metric in use is P/PET, instead of P. An additional promising feature is that Sulfur Injection can lead to a more rapid response in the next few decades, while the benefit is only gradually getting stronger in the case of Carbon Capture despite an earlier effort to lower the emission. Even though the mitigation of the two approaches are both introduced in around 2020 in these two experiments, the short-term (next 30 years) effect is stronger in the case of Sulfur Injection migration. The response time difference is due to the short-lived nature of sulfate aerosols, which will respond to mitigation measures more rapidly than long-lived species of CO2. However, we also point out the weaker efficiency of reverting the Amazon drying due to the further precipitation shift away from deep tropics to extratropic in response to Sulfur Injection. Moreover, we show that at a per-degree-cooling basis, Sulfur Injection is less effective than Carbon Capture at offsetting the drying tendency globally and more so regionally over the Amazon (Figure 9, bottom row), again, because of the stronger precipitation suppression.

An important note should be made regarding the interpretation of the quantitative "benefits" presented. Because these two models have different climate sensitivities, the baseline warming induced by unchecked emissions growth is not at the same level. The WACCM warms faster, reaches the 2ºC level at earlier decades, and has higher end-of-century warming at 6ºC, compared to the CESM. Since the baseline warming is different for the two models at different decades, the climate "benefit" due to any mitigation measures shall also be interpreted in a relative sense, i.e., the fraction (%) of the projected change in the future that can be mitigated by the Carbon Capture or Sulfur Injection. For example, even if our results suggest Sulfur Injection can lead to 5-6ºC cooling while the Carbon Capture can lead to a 4-5ºC cooling, that does not quantitatively provide any constraints onto the strength of respective approaches.

We further note that the strength of each geoengineering approach, even when expressed in relative terms, is subject to the assumption of applied forcing/perturbation. For example, the climate "benefit" can be enhanced by applying a larger Sulfur Injection or deploying Carbon Capture by a greater amount or earlier. In fact, in an earlier project that conducted a similar Carbon Capture experiments (Sanderson et al., 2017), a weaker version of decarbonization was presented (by applying a smaller amount of emission cut and Carbon Capture), under which the temperature temporarily exceed the 2ºC level during the 21st century (i.e., "overshoot"), before falling back onto a stabilized 1.5ºC level.

As a result, we emphasize that the main purpose of this paper is not to examine the effectiveness of these two climate engineering schemes in terms of absolute values. Instead, we aim to highlight the physical mechanisms at play, especially when distinct between the two approaches (e.g., radiative balances and dynamic response). The notable distinction between the two approaches includes response time scales, the role of solar dimming at the surface, the shift of deep tropical rainfall. The direct physiological role of CO_2 is potentially important because the CO_2 level is not reduced in the Sulfur Injection approach. But this study, focusing on meteorological drivers of land aridity using P/PET, did not delve into the physiological effect of CO_2 on plant transpiration via stomatal closure, which also appears to be weak in these two models compared with other climate models (Swann et al., 2018).

The analytical framework established here will thus (1) help to understand the contrasting response in terms of spatial and temporal distribution, that goes beyond the specific regions highlighted here, and (2) provide broader insights to the mitigation impact of other geoengineering approaches beyond the two discussed here (such as cirrus ice cloud thinning or marine warm cloud brightening, Muri et al., 2018; and surface albedo modifications, Crook et al., 2015; space mirror, Niemeier et al., 2013).

The quantitative results here using a suite of climate models thus need to be interpreted through the lens of model diversity. A recent example of such an attempt using two global climate models (Laakso et al., in review) focused on global-mean

precipitation response to carbon extraction and sulfur injection. Some aspects of the simulated responses here (e.g., the weaker sensitivity of precipitation to Sulfur Injection in WACCM) are worth revisiting by conducting systematic experiments using other climate models, such as the newly available CESM2 (WACCM6). To place the two types of geoengineering schemes in a broader context, future research is also needed to further examine the upcoming model output from the GeoMIP6 (The Geoengineering Model Intercomparison Project Phase 6) and CDRMIP.

References

Bala G., P. B. Duffy, and K. E. Taylor, 2008: Impact of geoengineering schemes on the global hydrological cycle, Proceeding of the National Academy of Sciences, 105(22), 7664-7669

Bala, G., K. Calderia, R. Nemani, 2009: Fast versus slow response in climate change: Implication to the global hydrological cycle, Climate Dynamics, DOI 10.1007/s00382-009-0583-y

Cao, L., Duan, L., Bala, G. and Caldeira, K.: Simultaneous stabilization of global temperature and precipitation through cocktail geoengineering, Geophys. Res. Lett., 44(14), 7429–7437, doi:10.1002/2017GL074281, 2017.

Chen, M., Xie, P., Janowiak, J. E. and Arkin, P. A.: Global Land Precipitation: A 50-yr Monthly Analysis Based on Gauge Observations, J. Hydrometeorol., 3(3), 249–266, doi:10.1175/1525-7541(2002)003<0249:GLPAYM>2.0.CO;2, 2002.

Cheng, W., MacMartin, D. G., Dagon, K., Kravitz, B., Tilmes, S., Richter, J. H., Mills, M. J. and Simpson, I. R.: Soil Moisture and Other Hydrological Changes in a Stratospheric Aerosol Geoengineering Large Ensemble, J. Geophys. Res. Atmos., 124(23), 12773–12793, doi:10.1029/2018JD030237, 2019.

Crook, J. A., Jackson, L. S., Osprey, S. M. and Forster, P. M.: A comparison of temperature and precipitation responses to different Earth radiation management geoengineering schemes, J. Geophys. Res. Atmos., 120(18), 9352–9373, doi:10.1002/2015JD023269, 2015.

Crutzen, P. J.: Albedo Enhancement by Stratospheric Sulfur Injections: A Contribution to Resolve a Policy Dilemma?, Clim. Change, 77(3–4), 211–220, doi:10.1007/s10584-006-9101-y, 2006.

Dai, A.: Characteristics and trends in various forms of the Palmer Drought Severity Index during 1900–2008, J. Geophys. Res., 116(D12), D12115, doi:10.1029/2010JD015541, 2011.

Duan, Long Cao, G. Bala and K. Caldeira, 2018: Comparison of the Fast and Slow Climate Response to Three Radiation Management Geoengineering Schemes, J. Geophys. Res. -Atmos., 10.1029/2018JD029034

Donat, M. G., Alexander, L. V, Yang, H., Durre, I., Vose, R., Dunn, R. J. H., Willett, K. M., Aguilar, E., Brunet, M., Caesar, J., Hewitson, B., Jack, C., Klein Tank, A. M. G., Kruger, A. C., Marengo, J., Peterson, T. C., Renom, M., Oria Rojas, C., Rusticucci, M., Salinger, J., Elrayah, A. S., Sekele, S. S., Srivastava, A. K., Trewin, B., Villarroel, C., Vincent, L. A., Zhai, P.,

Zhang, X. and Kitching, S.: Updated analyses of temperature and precipitation extreme indices since the beginning of the twentieth century: The HadEX2 dataset, J. Geophys. Res. Atmos., 118(5), 2098–2118, doi:10.1002/jgrd.50150, 2013.

Easterling, D. R.: Climate Extremes: Observations, Modeling, and Impacts, Science (80-.)., 289(5487), 2068–2074, doi:10.1126/science.289.5487.2068, 2000.

Effiong, U. and Neitzel, R. L.: Assessing the direct occupational and public health impacts of solar radiation management with stratospheric aerosols, Environ. Heal., 15(1), 7, doi:10.1186/s12940-016-0089-0, 2016.

Fan, Y. and van den Dool, H.: A global monthly land surface air temperature analysis for 1948–present, J. Geophys. Res., 113(D1), D01103, doi:10.1029/2007JD008470, 2008.

Feng, S. and Fu, Q.: Expansion of global drylands under a warming climate, Atmos. Chem. Phys., 13(19), 10081–10094, doi:10.5194/acp-13-10081-2013, 2013.

Fischer, E. M. and Knutti, R.: Anthropogenic contribution to global occurrence of heavy-precipitation and high-temperature extremes, Nat. Clim. Chang., 5(6), 560–564, doi:10.1038/nclimate2617, 2015.

Fu, Q. and Feng, S.: Responses of terrestrial aridity to global warming, J. Geophys. Res. Atmos., 119(13), 7863–7875, doi:10.1002/2014JD021608, 2014.

Giorgi, F., Coppola, E. and Raffaele, F.: A consistent picture of the hydroclimatic response to global warming from multiple indices: Models and observations, J. Geophys. Res. Atmos., 119(20), 11,695-11,708, doi:10.1002/2014JD022238, 2014.

Gettelman, A., Mills, M. J., Kinnison, D. E., Garcia, R. R., Smith, A. K., Marsh, D. R., et al. (2019). The whole atmosphere community climate model version 6 (WACCM6). Journal of Geophysical Research: Atmospheres, 124, 12380– 12403. https://doi.org/10.1029/2019JD030943

Helwegen, K. G., Wieners, C. E., Frank, J. E. and Dijkstra, H. A.: Complementing CO 2 emission reduction by solar radiation management might strongly enhance future welfare, Earth Syst. Dyn., 10(3), 453–472, doi:10.5194/esd-10-453-2019, 2019.

Herzog, H. J.: Peer Reviewed: What Future for Carbon Capture and Sequestration?, Environ. Sci. Technol., 35(7), 148A-153A, doi:10.1021/es012307j, 2001.

Hu, A., Xu, Y., Tebaldi, C., Washington, W. M. and Ramanathan, V.: Mitigation of short-lived climate pollutants slows sea-level rise, Nat. Clim. Chang., 3(8), 730–734, doi:10.1038/nclimate1869, 2013.

Huang, J., Li, Y., Fu, C., Chen, F., Fu, Q., Dai, A., Shinoda, M., Ma, Z., Guo, W., Li, Z., Zhang, L., Liu, Y., Yu, H., He, Y., Xie, Y., Guan, X., Ji, M., Lin, L., Wang, S., Yan, H. and Wang, G.: Dryland climate change: Recent progress and challenges, Rev. Geophys., 55(3), 719–778, doi:10.1002/2016RG000550, 2017.

Irvine, P. J., Kravitz, B., Lawrence, M. G., Gerten, D., Caminade, C., Gosling, S. N., Hendy, E. J., Kassie, B. T., Kissling, W. D., Muri, H., Oschlies, A. and Smith, S. J.: Towards a comprehensive climate impacts assessment of solar geoengineering, Earth's Futur., 5(1), 93–106, doi:10.1002/2016EF000389, 2017.

Keller, D. P., Feng, E. Y. and Oschlies, A.: Potential climate engineering effectiveness and side effects during a high carbon dioxide-emission scenario, Nat. Commun., 5(1), 3304, doi:10.1038/ncomms4304, 2014.

Kleidon, A., Kravitz, B. and Renner, M.: The hydrological sensitivity to global warming and solar geoengineering derived from thermodynamic constraints, Geophys. Res. Lett., 42(1), 138–144, doi:10.1002/2014GL062589, 2015.

Knapp, A. K., Beier, C., Briske, D. D., Classen, A. T., Luo, Y., Reichstein, M., Smith, M. D., Smith, S. D., Bell, J. E., Fay, P. A., Heisler, J. L., Leavitt, S. W., Sherry, R., Smith, B. and Weng, E.: Consequences of More Extreme Precipitation Regimes for Terrestrial Ecosystems, Bioscience, 58(9), 811–821, doi:10.1641/B580908, 2008.

Kravitz, B., MacMartin, D. G., Mills, M. J., Richter, J. H., Tilmes, S., Lamarque, J.-F., Tribbia, J. J. and Vitt, F.: First Simulations of Designing Stratospheric Sulfate Aerosol Geoengineering to Meet Multiple Simultaneous Climate Objectives, J. Geophys. Res. Atmos., 122(23), 12,616-12,634, doi:10.1002/2017JD026874, 2017.

Kravitz, B., Robock, A. and Irvine, P.: Robust Results From Climate Model Simulations of Geoengineering, Eos, Trans. Am. Geophys. Union, 94(33), 292–292, doi:10.1002/2013EO330005, 2013.

Kunkel, K. E., Pielke, R. A. and Changnon, S. A.: Temporal Fluctuations in Weather and Climate Extremes That Cause Economic and Human Health Impacts: A Review, Bull. Am. Meteorol. Soc., 80(6), 1077–1098, doi:10.1175/1520-0477(1999)080<1077:TFIWAC>2.0.CO;2, 1999.

Lawrence, M. G., Schäfer, S., Muri, H., Scott, V., Oschlies, A., Vaughan, N. E., Boucher, O., Schmidt, H., Haywood, J. and Scheffran, J.: Evaluating climate geoengineering proposals in the context of the Paris Agreement temperature goals, Nat. Commun., 9(1), 3734, doi:10.1038/s41467-018-05938-3, 2018.

Lesk, C., Rowhani, P. and Ramankutty, N.: Influence of extreme weather disasters on global crop production, Nature, 529(7584), 84–87, doi:10.1038/nature16467, 2016.

Lin, L., Wang, Z., Xu, Y., Zhang, X., Zhang, H. and Dong, W.: Additional Intensification of Seasonal Heat and Flooding Extreme Over China in a 2°C Warmer World Compared to 1.5°C, Earth's Futur., 6(7), 968–978, doi:10.1029/2018EF000862, 2018.

MacMartin, D. G., Kravitz, B., Tilmes, S., Richter, J. H., Mills, M. J., Lamarque, J.-F., Tribbia, J. J. and Vitt, F.: The Climate Response to Stratospheric Aerosol Geoengineering Can Be Tailored Using Multiple Injection Locations, J. Geophys. Res. Atmos., 122(23), 12,574-12,590, doi:10.1002/2017JD026868, 2017.

MacMartin, D. G., Ricke, K. L. and Keith, D. W.: Solar geoengineering as part of an overall strategy for meeting the 1.5°C Paris target, Philos. Trans. R. Soc. A Math. Phys. Eng. Sci., 376(2119), 20160454, doi:10.1098/rsta.2016.0454, 2018.

Meinshausen, M., Meinshausen, N., Hare, W., Raper, S. C. B., Frieler, K., Knutti, R., Frame, D. J. and Allen, M. R.: Greenhouse-gas emission targets for limiting global warming to 2 °C, Nature, 458(7242), 1158–1162, doi:10.1038/nature08017, 2009.

Mills, M. J., Richter, J. H., Tilmes, S., Kravitz, B., MacMartin, D. G., Glanville, A. A., Tribbia, J. J., Lamarque, J.-F., Vitt, F., Schmidt, A., Gettelman, A., Hannay, C., Bacmeister, J. T. and Kinnison, D. E.: Radiative and Chemical Response to Interactive Stratospheric Sulfate Aerosols in Fully Coupled CESM1(WACCM), J. Geophys. Res. Atmos., 122(23), 13,061-13,078, doi:10.1002/2017JD027006, 2017.

Mishra, A. K. and Singh, V. P.: A review of drought concepts, J. Hydrol., 391(1–2), 202–216, doi:10.1016/j.jhydrol.2010.07.012, 2010.

Moore, J. C., Rinke, A., Yu, X., Ji, D., Cui, X., Li, Y., Alterskjaer, K., Kristjánsson, J. E., Muri, H., Boucher, O., Huneeus, N., Kravitz, B., Robock, A., Niemeier, U., Schulz, M., Tilmes, S., Watanabe, S. and Yang, S.: Arctic sea ice and atmospheric circulation under the GeoMIP G1 scenario, J. Geophys. Res. Atmos., 119(2), 567–583, doi:10.1002/2013JD021060, 2014.

Muri, H., Tjiputra, J., Otterå, O. H., Adakudlu, M., Lauvset, S. K., Grini, A., Schulz, M., Niemeier, U. and Kristjánsson, J. E.: Climate Response to Aerosol Geoengineering: A Multimethod Comparison, J. Clim., 31(16), 6319–6340, doi:10.1175/JCLI-D-17-0620.1, 2018.

Niemeier, U. and Tilmes, S.: Sulfur injections for a cooler planet, Science (80-.)., 357(6348), 246–248, doi:10.1126/science.aan3317, 2017.

Niemeier, U., Schmidt, H., Alterskjær, K., and Kristjánsson, J. E. (2013), Solar irradiance reduction via climate engineering: Impact of different techniques on the energy balance and the hydrological cycle, J. Geophys. Res. Atmos., 118, 11,905– 11,917

Peters, G. P., Andrew, R. M., Boden, T., Canadell, J. G., Ciais, P., Le Quéré, C., Marland, G., Raupach, M. R. and Wilson, C.: The challenge to keep global warming below 2 °C, Nat. Clim. Chang., 3(1), 4–6, doi:10.1038/nclimate1783, 2013.

Pongratz, J., Lobell, D. B., Cao, L. and Caldeira, K.: Crop yields in a geoengineered climate, Nat. Clim. Chang., 2(2), 101–105, doi:10.1038/nclimate1373, 2012.

Porada, P., Weber, B., Elbert, W., Pöschl, U. and Kleidon, A.: Estimating impacts of lichens and bryophytes on global biogeochemical cycles, Global Biogeochem. Cycles, 28(2), 71–85, doi:10.1002/2013GB004705, 2014.

Richter, J. H., Tilmes, S., Mills, M. J., Tribbia, J. J., Kravitz, B., MacMartin, D. G., Vitt, F. and Lamarque, J.-F.: Stratospheric Dynamical Response and Ozone Feedbacks in the Presence of SO 2 Injections, J. Geophys. Res. Atmos., 122(23), 12,557-12,573, doi:10.1002/2017JD026912, 2017.

Richter, J. H., Tilmes, S., Glanville, A., Kravitz, B., MacMartin, D. G., Mills, M. J., Simpson, I. R., Vitt, F., Tribbia, J. J. and Lamarque, J.-F.: Stratospheric Response in the First Geoengineering Simulation Meeting Multiple Surface Climate Objectives, J. Geophys. Res. Atmos., 123(11), 5762–5782, doi:10.1029/2018JD028285, 2018.

Field, L., Ivanova, D., Bhattacharyya, S., Mlaker, V., Sholtz, A., Decca, R., et al. (2018). Increasing Arctic sea ice albedo using localized reversible geoengineering. Earth's Future, 6, 882–901. https:// doi.org/10.1029/2018EF000820

Robock, A., Marquardt, A., Kravitz, B. and Stenchikov, G.: Benefits, risks, and costs of stratospheric geoengineering, Geophys. Res. Lett., 36(19), L19703, doi:10.1029/2009GL039209, 2009.

Rodell, M., Houser, P. R., Jambor, U., Gottschalck, J., Mitchell, K., Meng, C.-J., Arsenault, K., Cosgrove, B., Radakovich, J., Bosilovich, M., Entin, J. K., Walker, J. P., Lohmann, D. and Toll, D.: The Global Land Data Assimilation System, Bull. Am. Meteorol. Soc., 85(3), 381–394, doi:10.1175/BAMS-85-3-381, 2004.

Salter, Stephen. "Spray turbines to increase rain by enhanced evaporation from the sea." Tenth Congress of International Maritime Association of the Mediterranean, Crete. 2002

Scheff, J. and Frierson, D. M. W.: Scaling Potential Evapotranspiration with Greenhouse Warming, J. Clim., 27(4), 1539–1558, doi:10.1175/JCLI-D-13-00233.1, 2014.

Schiermeier, Q.: Increased flood risk linked to global warming, Nature, 470(7334), 316–316, doi:10.1038/470316a, 2011.

Seager, R., Feldman, J., Lis, N., Ting, M., Williams, A. P., Nakamura, J., Liu, H. and Henderson, N.: Whither the 100th Meridian? The Once and Future Physical and Human Geography of America's Arid–Humid Divide. Part II: The Meridian Moves East, Earth Interact., 22(5), 1–24, doi:10.1175/EI-D-17-0012.1, 2018.

Seneviratne, S. I., Phipps, S. J., Pitman, A. J., Hirsch, A. L., Davin, E. L., Donat, M. G., Hirschi, M., Lenton, A., Wilhelm, M. and Kravitz, B.: Land radiative management as contributor to regional-scale climate adaptation and mitigation, Nat. Geosci., 11(2), 88–96, doi:10.1038/s41561-017-0057-5, 2018.

Seneviratne, S. I., Corti, T., Davin, E. L., Hirschi, M., Jaeger, E. B., Lehner, I., Orlowsky, B. and Teuling, A. J.: Investigating soil moisture–climate interactions in a changing climate: A review, Earth-Science Rev., 99(3–4), 125–161, doi:10.1016/j.earscirev.2010.02.004, 2010.

Shindell, D., Kuylenstierna, J. C. I., Vignati, E., van Dingenen, R., Amann, M., Klimont, Z., Anenberg, S. C., Muller, N., Janssens-Maenhout, G., Raes, F., Schwartz, J., Faluvegi, G., Pozzoli, L., Kupiainen, K., Hoglund-Isaksson, L., Emberson, L., Streets, D., Ramanathan, V., Hicks, K., Oanh, N. T. K., Milly, G., Williams, M., Demkine, V. and Fowler, D.: Simultaneously Mitigating Near-Term Climate Change and Improving Human Health and Food Security, Science (80-.)., 335(6065), 183–189, doi:10.1126/science.1210026, 2012.

Simpson, I. R., Tilmes, S., Richter, J. H., Kravitz, B., MacMartin, D. G., Mills, M. J., Fasullo, J. T. and Pendergrass, A. G.: The Regional Hydroclimate Response to Stratospheric Sulfate Geoengineering and the Role of Stratospheric Heating, J. Geophys. Res. Atmos., 124(23), 12587–12616, doi:10.1029/2019JD031093, 2019.

Tilmes, S., Sanderson, B. M. and O'Neill, B. C.: Climate impacts of geoengineering in a delayed mitigation scenario, Geophys. Res. Lett., 43(15), 8222–8229, doi:10.1002/2016GL070122, 2016.

Tilmes, S., Richter, J. H., Kravitz, B., MacMartin, D. G., Mills, M. J., Simpson, I. R., Glanville, A. S., Fasullo, J. T., Phillips, A. S., Lamarque, J.-F., Tribbia, J., Edwards, J., Mickelson, S. and Ghosh, S.: CESM1(WACCM) Stratospheric Aerosol Geoengineering Large Ensemble Project, Bull. Am. Meteorol. Soc., 99(11), 2361–2371, doi:10.1175/BAMS-D-17-0267.1, 2018.

Tilmes, S., Richter, J. H., Mills, M. J., Kravitz, B., MacMartin, D. G., Garcia, R. R., Kinnison, D. E., Lamarque, J.-F., Tribbia, J. and Vitt, F.: Effects of Different Stratospheric SO 2 Injection Altitudes on Stratospheric Chemistry and Dynamics, J. Geophys. Res. Atmos., 123(9), 4654–4673, doi:10.1002/2017JD028146, 2018.

Tilmes, S., Richter, J. H., Mills, M. J., Kravitz, B., MacMartin, D. G., Vitt, F., Tribbia, J. J. and Lamarque, J.-F.: Sensitivity of Aerosol Distribution and Climate Response to Stratospheric SO 2 Injection Locations, J. Geophys. Res. Atmos., 122(23), 12,591-12,615, doi:10.1002/2017JD026888, 2017.

Vaughan, N. E. and Lenton, T. M.: A review of climate geoengineering proposals, Clim. Change, 109(3–4), 745–790, doi:10.1007/s10584-011-0027-7, 2011.

Victor, D. G., Zaelke, D. and Ramanathan, V.: Soot and short-lived pollutants provide political opportunity, Nat. Clim. Chang., 5(9), 796–798, doi:10.1038/nclimate2703, 2015.

Wang, Z., Lin, L., Yang, M., Xu, Y., and J. Li, (2017) Disentangling fast and slow responses of the East Asian summer monsoon to reflecting and absorbing aerosol forcings, Atmos. Chem. Phys., 17, 11075-11088, https://doi.org/10.5194/acp-17-11075-2017.

Wang, Z., Lin, L., Zhang, X., Zhang, H., Liu, L. and Xu, Y.: Scenario dependence of future changes in climate extremes under 1.5 °C and 2 °C global warming, Sci. Rep., 7(1), 46432, doi:10.1038/srep46432, 2017.

Wigley, T. M. L.: A Combined Mitigation/Geoengineering Approach to Climate Stabilization, Science (80-.)., 314(5798), 452–454, doi:10.1126/science.1131728, 2006.

Xu, Y., and V. Ramanathan (2017), Well below 2 °C: Mitigation strategies for avoiding dangerous to catastrophic climate changes. Proc. Natl. Acad. Sci. , doi:10.1073/pnas.1618481114 .

Tables

Table 1. The model experiments.

Experiment short name	Model	Simulation period	Ensemble size	Reference
CESM_Historical	CESM1-CAM5	1975-2005	30	Kay et al., 2015
CESM_RCP8.5	CESM1-CAM5	2006-2099	30	Kay et al., 2015
CESM_CarbonCapture	CESM1-CAM5	2006-2099	10	Sanderson et al., 2017
WACCM_RCP8.5	CESM1-WACCM	2010-2099	20 before 2030, 3 after 2030	Tilmes et al., 2018
WACCM_SulfurInjection	CESM1-WACCM	2020-2099	20	Tilmes et al., 2018

Table 2. The changes in key hydroclimate variables (bias-corrected based on observation) over "Major Land" (60ºS to 60ºN). All numbers are derived from the time series in Figure 3. All changes are statistically significant at the 95% level. The definition of "major land" is the land regions over 60ºS to 60ºN, thus excluding cold regions where the seasonal snow cover or permanent ice sheet surface makes P/PET less useful as a predictor for aridity and vegetation types. The focused periods are Present-day: 2010-2019; Mid-century: 2046-2055; End of century: 2086-2095. Values in the parentheses are percentage relative to present-day levels. The uncertainty estimate based on the large ensemble spread (one standard deviation) after the "±".

Variables	T (ºC)		P (mm/year)		PET (mm/year)		P/PET (unitless)	
Time periods	Mid-century	End of century	Mid-century	End of century	Mid-century	End of century	Mid-century	End of century
Changes under RCP8.5 by CESM (percentage relative to present-day)	2.0±0.3	4.5±0.3	23.0±24.0 (2.9±3.1%)	59.2±32.4 (7.6±4.2%)	93.2±13.9 (7.5±1.1%)	229.1±15.2 (18.5±1.2%)	-0.03±0.02 (-4.2±3.2%)	-0.06±0.02 (-9.2±3.8%)
Changes under RCP8.5 by WACCM (percentage relative to present-day)	2.5±0.3	5.8±0.4	54.2±40.5 (7.0±5.2%)	123.2±57.9 (15.8±7.4%)	103.8±14.5 (8.4±1.2%)	249.4±14.6 (20.1±1.2%)	-0.01±0.03 (-1.3±5.3%)	-0.02±0.04 (-3.6±6.3%)
CarbonCapture benefits (percentage relative to CESM_RCP8.5)	-1.3±0.1	-4.0±0.1	-7.1±6.4 (-0.4±0.8%)	-36.8±5.5 (-4.2±0.7%)	-55.4±4.5 (-3.9±0.4%)	-188.8±3.3 (-14.6±0.3%)	0.02±0.01 (3.2±1.1%)	0.06±0.01 (8.8±0.9%)
SulfurInjection benefits (percentage relative to WACCM_RCP8.5)	-2.4±0.1	-5.7±0.1	-40.4±8.6 (-5.2±1.1%)	-121.0±7.9	-128.0±3.0 (-10.3±0.2%)	-289.5±3.9	0.03±0.01 (5.1±1.1%)	0.05±0.01 (7.2±1.2%)

				(-15.5±1.0%)		(-23.3±0.3%)		

Table 3. Dryland area (million km^2) for semi-arid/arid types. North America is 15ºN-60ºN and 230ºE-300ºE. South America is 60ºS-10ºN and 280ºE-330ºE.

semi-arid/arid area (km^2)	Global Major Land	North America	South America
CESM_Historical (after bias-correction, 1975-2005)	20.4/15.0	3.3/0.8	1.8/0.5
CESM_RCP8.5 (2086-2095)	22.9/16.6	3.9/1.2	2.1/0.6
CESM_CarbonCapture (2086-2095)	20.7/15.1	3.4/0.7	1.8/0.5
WACCM_RCP8.5 (2086-2095)	24.3/15.5	4.0/1.3	1.8/0.8
WACCM_SulfurInjection (2086-2095)	21.8/13.5	3.2/0.6	1.7/0.5

Table 4. Global major land changes in P, PET, and P/PET, normalized by global temperature change. Two methods are used here: The first method is comparing the epoch difference of the end-of-century climate to obtain the normalized response. The second method is conducting linear regression over the decadal time series of anomaly induced by Carbon Capture or Sulfur Injection. In the rightmost columns, we contrast the results with the response to atmospheric CO2, tropospheric SO4 in the 20th century, as well as the various forcing experiments in the Last Millennium Ensemble (LME). The values after the "±" is one standard deviation.

P (%/ºC)	Carbon Capture	Sulfur Injection	CO2 (Lin et al., 2016a)	Trop. SO2 (Lin et al., 2016a)	LME GHG	LME O3&AER	LME Volcanic 1250-1270/ 1450-1460/ 1800-1820
Epoch difference	1.1±1.9	2.4±2.2	1.2±0.4	6.7±1.5	1.4±2.3	8.1±2.9	2.6±12.0 /4.1±7.9 / 2.5±10.0
Linear regression	1.1±0.9	2.7±3.3	n/a	n/a	n/a	n/a	n/a

PET (%/ºC)	Carbon Capture	Sulfur Injection	CO2 (Lin et al., 2016a)	Trop. SO2 (Lin et al., 2016a)	LME GHG	LME O3&AER	LME Volcanic 1250-1270/ 1450-1460/ 1800-1820
Epoch difference	3.5±2.9	4.0±2.1	4.6±0.2	6.3±0.4	4.2±	7.7±	7.2±10.8 / 6.4±6.8 / 5.6±6.9
Linear regression	3.8±0.3	4.0±0.4	n/a	n/a	n/a	n/a	n/a

P/PET (%/ºC)	Carbon Capture	Sulfur Injection	CO2 (Lin et al., 2016a)	Trop. SO2 (Lin et al., 2016a)	LME GHG	LME O3&AER	LME Volcanic 1250-1270/ 1450-1460/ 1800-1820
Epoch difference	-2.0±2.0	-1.5±1.7	-3.3±0.5	0.4±1.6	-2.7±2.6	0.3±4.1	-4.9±10.4 /-2.5±7.2 /-3.2±9.3
Linear regression	-2.2±1.0	-1.1±3.1	n/a	n/a	n/a	n/a	n/a

Table 5. Change (%/℃) in PET, and P/PET due to contributions of other climate variables (RH2M, U10, T, Rn-G, P). The variables used for this table are not bias-corrected because of the lack of reliable benchmark for U10 and Rn-G (surface available energy, which is the incoming radiation reaching the ground minus the heat flux into the ground).

(a) Contribution to PET change

Carbon Capture / Sulfur Injection (%/℃)	RH2M (relative humidity at 2 meter)	U10 (surface wind at 10 meter)	T	Rn-G (surface available energy)
Global major land	0.7 / 0.4	0.1 / 0.2	3.2 / 3.0	1.0 / 1.4
North Brazil	1.4 / 0.4	0.3 / 0.0	2.3 / 1.6	2.2 / 1.6
South Brazil	0.8 / 1.2	0.0 / 0.6	2.3 / 2.3	1.1 / 0.8

(b) Contribution to P/PET change

Carbon Capture / Sulfur Injection (%/℃)	RH2M (relative humidity)	U10 (surface wind)	T	Rn-G (surface available energy)	P
Global major land	-0.7 / -0.4	-0.1 / -0.2	-2.7 / -2.6	-0.8 / -1.3	1.7 / 3.0
North Brazil	-1.1 / -0.3	-0.2 / 0.0	-1.5 / -1.2	-1.6 / -1.3	**-3.4** / 0.9
South Brazil	-0.7 / -1.1	0.0 / -0.4	-1.9 / -1.8	-1.0 / -0.7	1.6 / **-1.0**

Figures

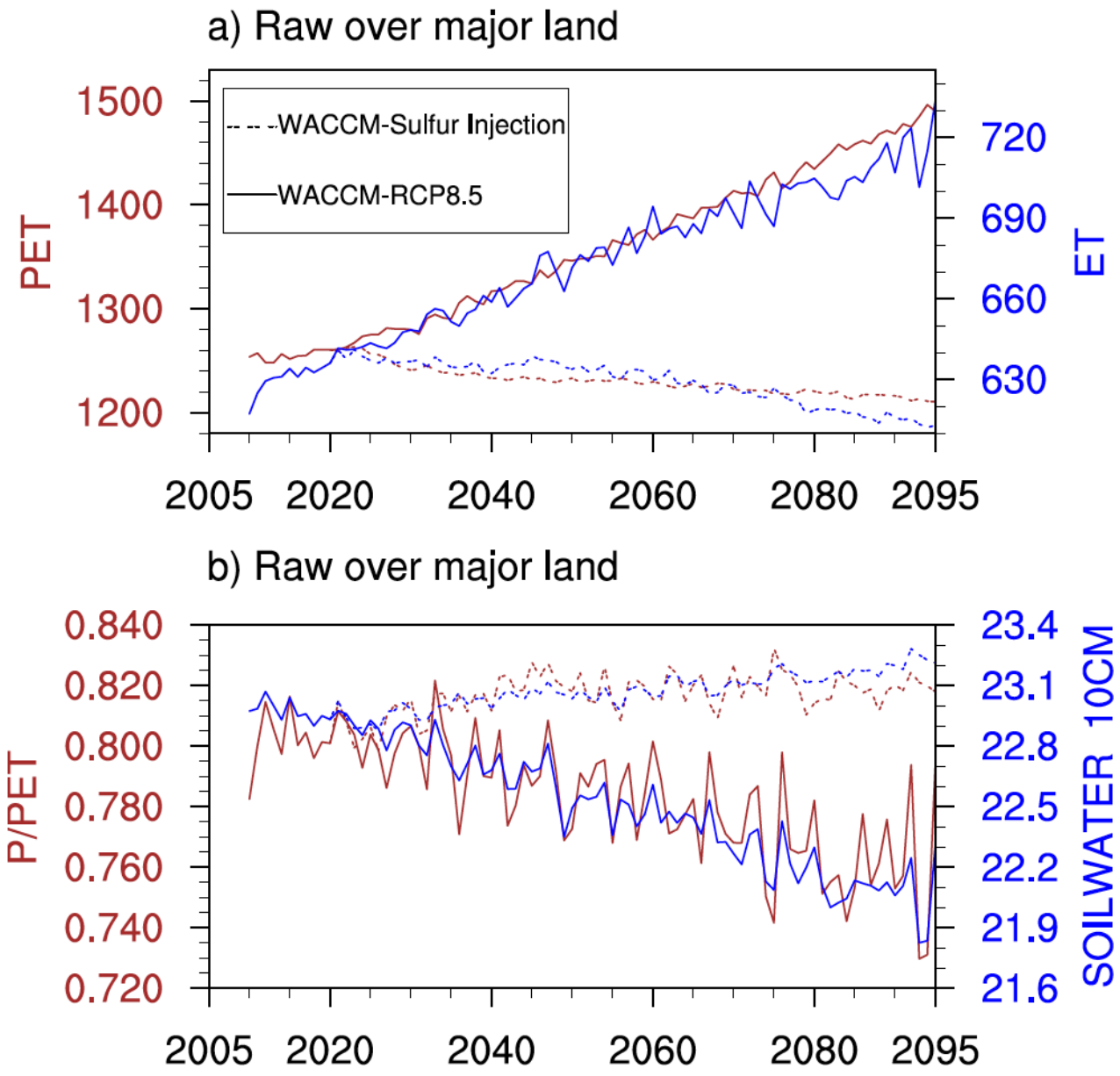

Figure 1. (a) PET (mm/year) and ET (mm/year) as simulated by WACCM, over global major land regions (60ºS to 60ºN) only, because P/PET is not a good indicator of drought condition over snow-covered cold regions. (b) P/PET (unitless) and soil water in the top 10cm layer (mm). The solid lines are for the left Y-axis and the dashed lines are for the right Y-axis. Red lines are under

RCP8.5 and blue lines are under Sulfur Injection. Note that no bias correction or smoothing was performed for this figure. CESM results are not shown because (a) there is no reduction of soil moisture in the RCP8.5 warming and (b) there is no separation of soil moisture in the long-term trends between the RCP8.5 and mitigated warming simulations, presumably due to model deficiency outside the Americas, because within Americas (Figure 2), the CESM results are largely consistent with WACCM.

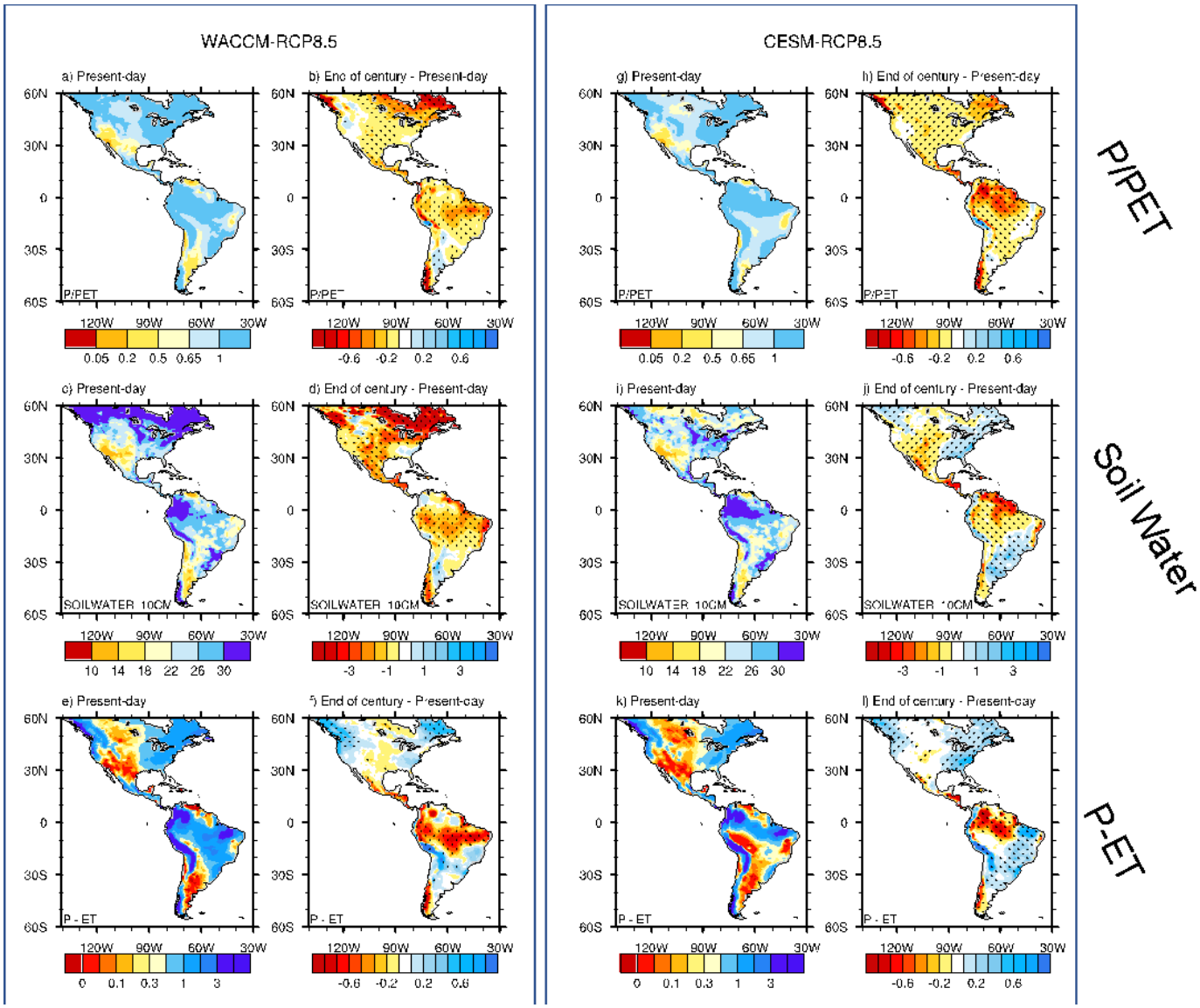

Figure 2. (Left two columns) WACCM simulated P/PET (unitless), soil water (mm), P-ET (mm/day), at the present day, and its end-of-century change under RCP8.5. (Right two columns) Same as left, but for CESM. Note that all data here in Figure 2 are without bias correction as in Figure 1. The focused periods are Present-day (2010-2019) and End-of-century (2086-2095). The areas with stippling in the panels of "End-of-Century – Present-day" are where the differences are significant at a 95% confidence level following the student's T-test. Similar results are presented in Figure 5 but after bias correction and in relative terms (%).

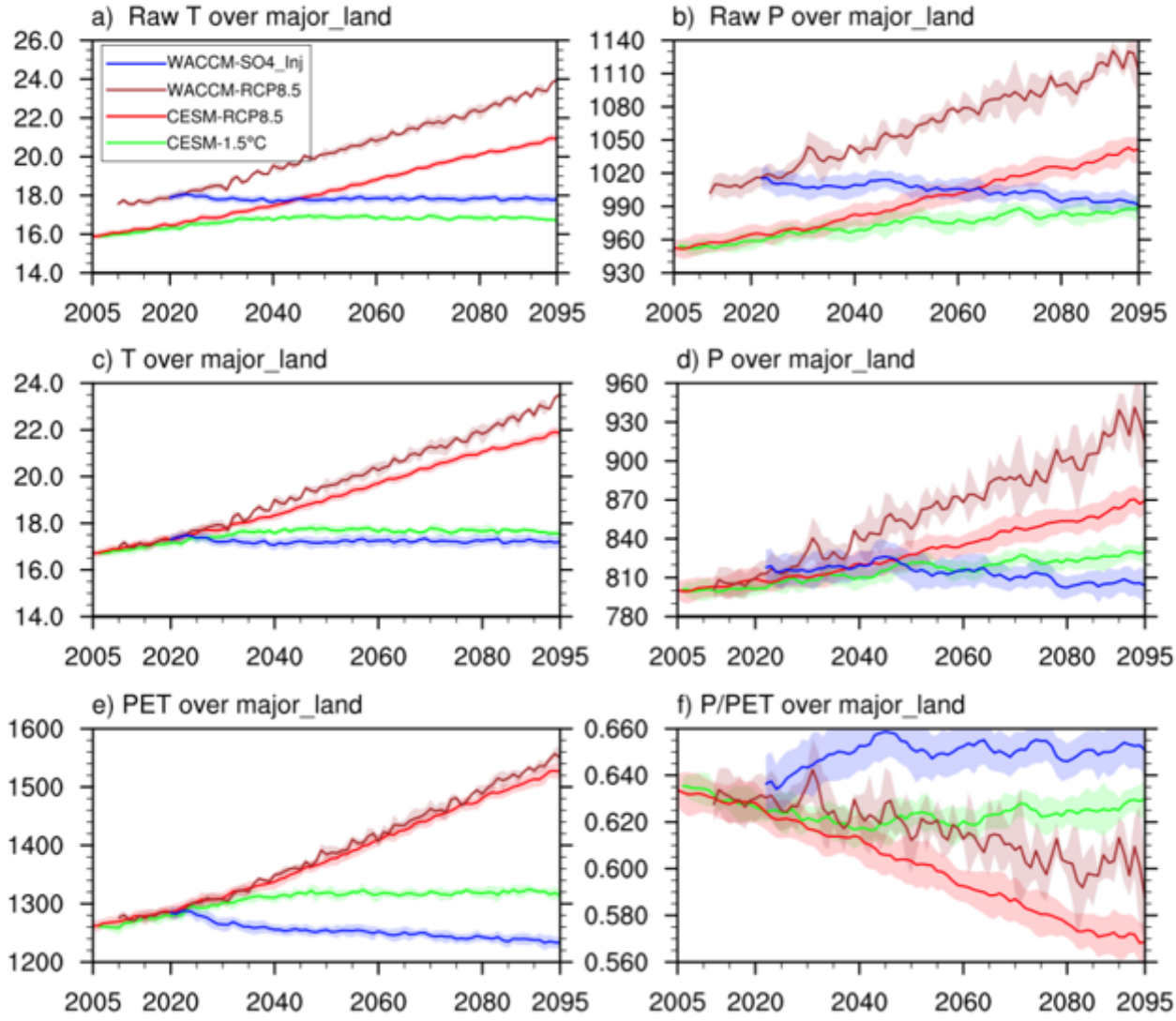

Figure 3. The annual average of major land temperature (T) (°C) (the first row without bias correction and the second row with bias correction), and major land precipitation (P) (mm/year) (the first row without bias correction and the second row with bias correction). The third row shows the major land PET (mm/year), and major land P/PET (unitless) (after bias correction). Shading represents the standard deviation of ensemble members. We have applied decadal smoothing to all the time series but note that WACCM-RCP8.5 has 3 ensemble members during 2030-2099, and thus has large fluctuation due to natural variation, in contrast with 10 or more ensemble members in other cases.

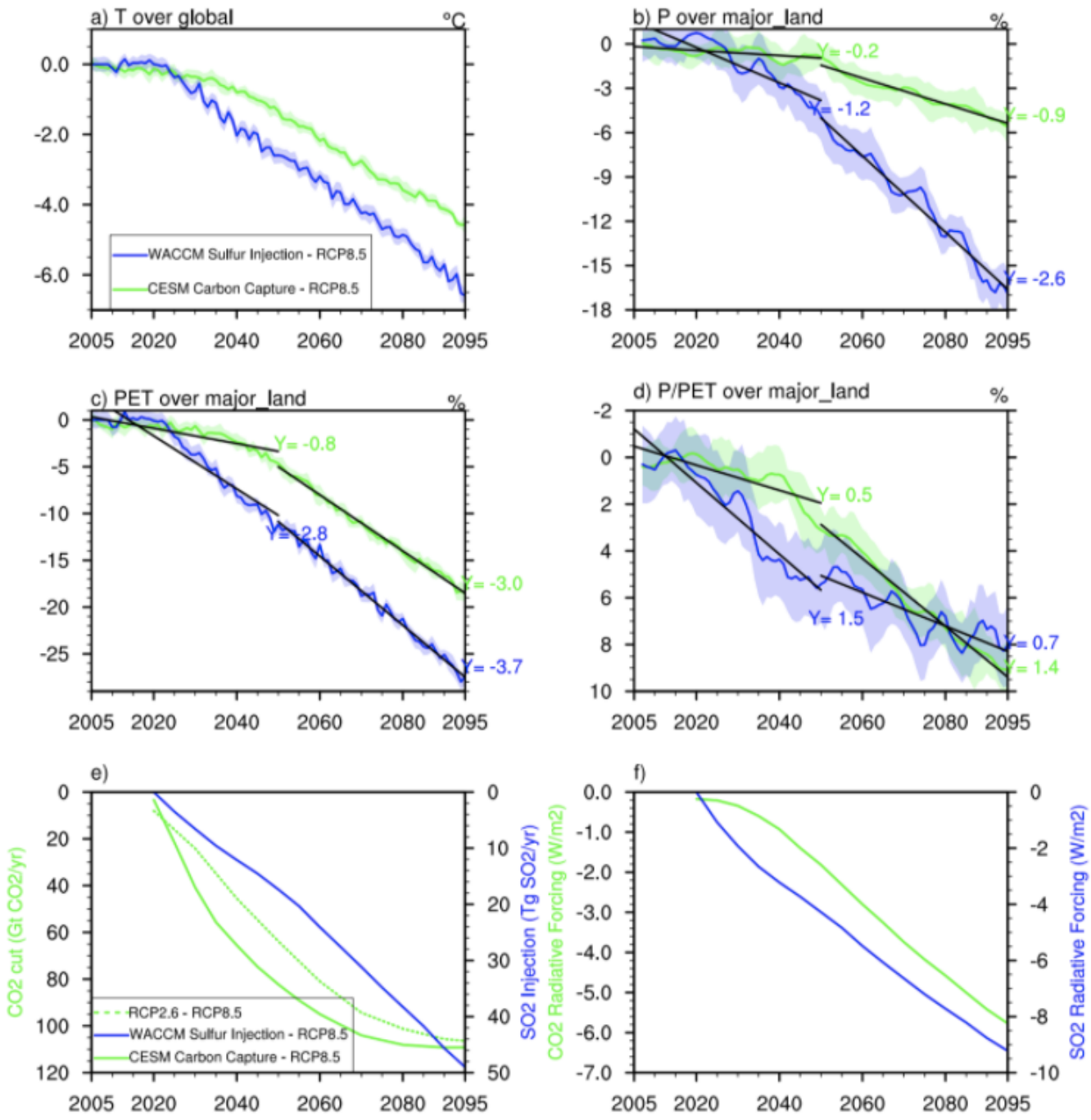
a) T over global
°C
0.0
-2.0
-4.0
-6.0
WACCM Sulfur Injection - RCP8.5
CESM Carbon Capture - RCP8.5
2005 2020 2040 2060 2080 2095
b) P over major_land
%
0
-3
-6
-9
-12
-15
-18
Y= -0.2
Y= -1.2
Y= -0.9
Y= -2.6
2005 2020 2040 2060 2080 2095
c) PET over major_land
%
0
-5
-10
-15
-20
-25
Y= -0.8
Y= -2.8
Y= -3.0
Y= -3.7
2005 2020 2040 2060 2080 2095
d) P/PET over major_land
%
-2
0
2
4
6
8
10
Y= 0.5
Y= 1.5
Y= 0.7
Y= 1.4
2005 2020 2040 2060 2080 2095
e)
CO2 cut (Gt CO2/yr)
SO2 Injection (Tg SO2/yr)
0
20
40
60
80
100
120
0
10
20
30
40
50
RCP2.6 - RCP8.5
WACCM Sulfur Injection - RCP8.5
CESM Carbon Capture - RCP8.5
2005 2020 2040 2060 2080 2095
f)
CO2 Radiative Forcing (W/m2)
SO2 Radiative Forcing (W/m2)
0.0
-1.0
-2.0
-3.0
-4.0
-5.0
-6.0
-7.0
0
-2
-4
-6
-8
-10
2005 2020 2040 2060 2080 2095

Figure 4. The changes of T, P, PET, and P/PET due to two types of geoengineering schemes. The changes are shown in relative terms (except for T in ºC), which is computed from the absolute values in Figure 3. In panel (d), the linear fit for the blue and green lines (separately for 2005-2050 and 2050-2095) is to highlight the near-term "benefit" of Sulfur Injection. (e) the mass of carbon cut (Gt CO2/yr) and sulfur injection (Tg SO2/yr). The dash green line is the RCP2.6 carbon cut for comparison; (f) the radiative forcing (W/m2) due to carbon capture and sulfate injection. The mass of carbon cut and corresponding radiative forcing is based on Figure 1 of Sanderson et al. (2017). The mass of sulfur injection comes from Figure 2 of Tilmes et al. (2018). The sulfate radiative forcing is calculated based on the equations in Metzner et al. (2012).

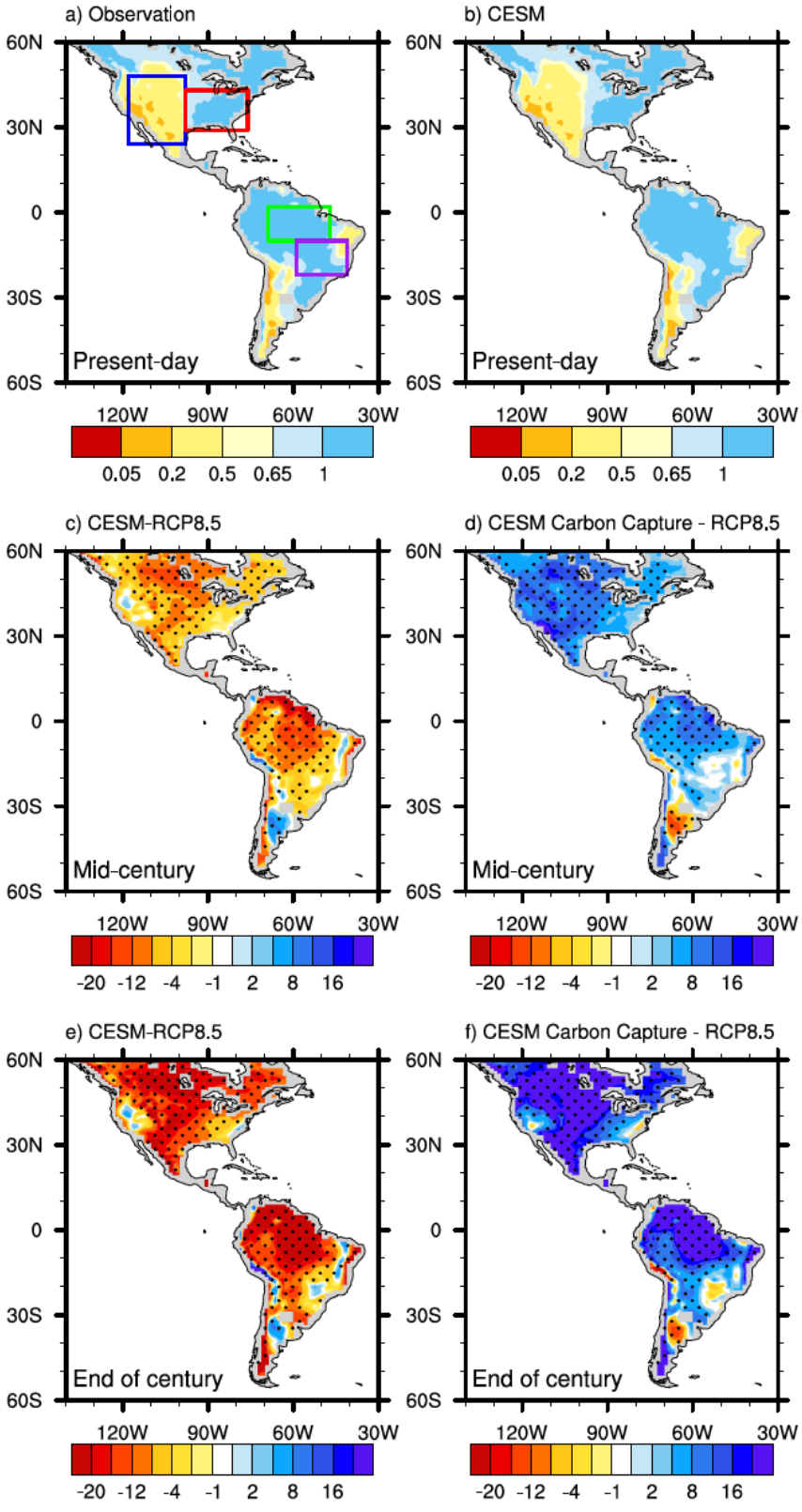
a) Observation
b) CESM
c) CESM-RCP8.5
d) CESM Carbon Capture - RCP8.5
e) CESM-RCP8.5
f) CESM Carbon Capture - RCP8.5
Present-day
Mid-century
End of century
60N
30N
0
30S
60S
120W
90W
60W
30W
0.05 0.2 0.5 0.65 1
-20 -12 -4 -1 2 8 16

Figure 5. P/PET in the present day, the relative changes (%) in the future under RCP8.5 and mitigation due to carbon capture geoengineering using CESM. The first row: the reanalysis and the bias-corrected output of the model at the present day (unitless). The second row: (c) The projected baseline changes relative to present-day (%); (d) The mitigation of the baseline changes relative to present-day. The third row: same as the second but for the end of the century. The similar P/PET changes in absolute values (unitless) can be found in row 1 of Figure 2.

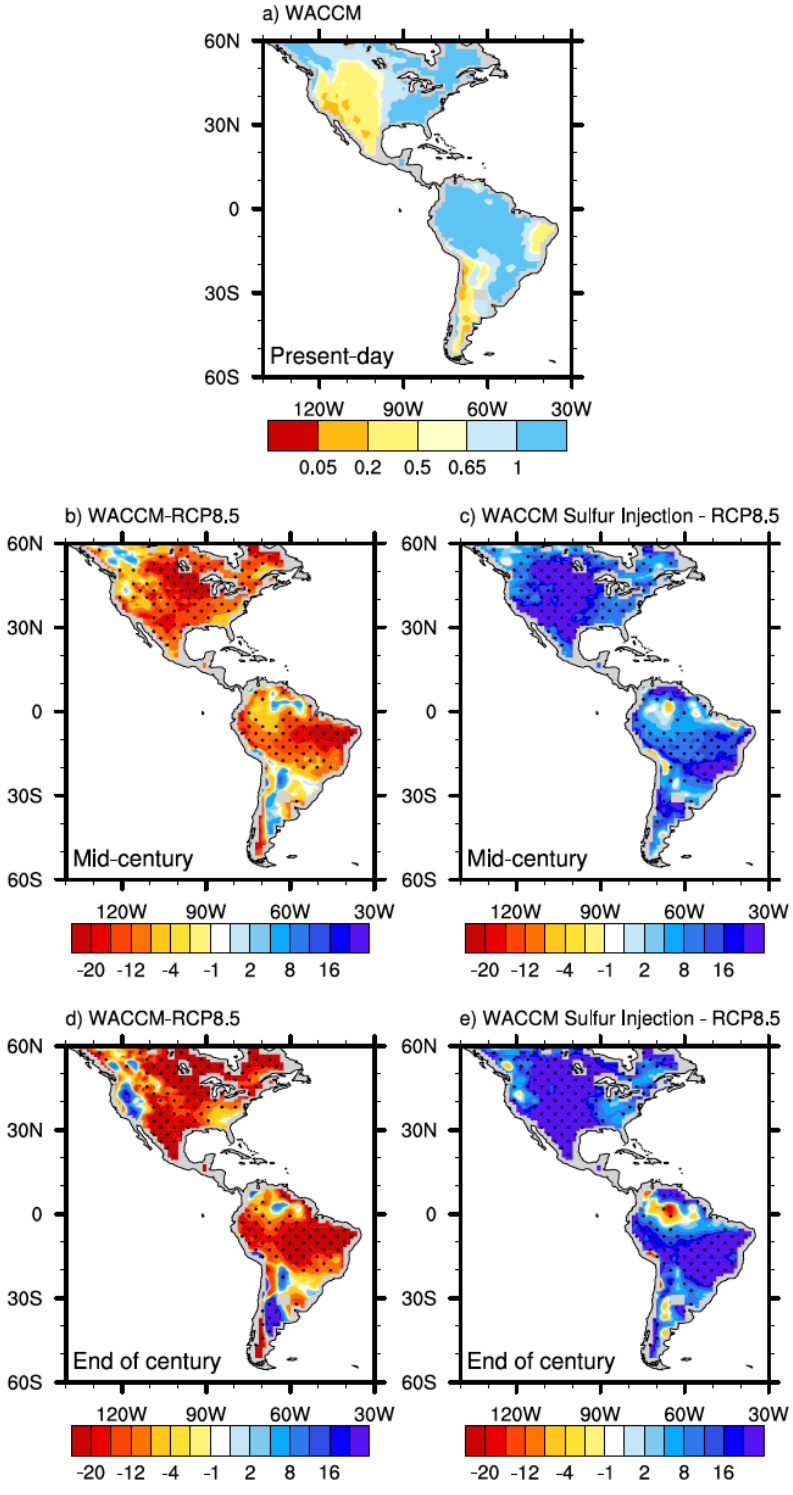
a) WACCM
60N
30N
0
30S
60S
Present-day
120W
90W
60W
30W
0.05 0.2 0.5 0.65 1
b) WACCM-RCP8.5
Mid-century
c) WACCM Sulfur Injection - RCP8.5
Mid-century
-20 -12 -4 -1 2 8 16
d) WACCM-RCP8.5
End of century
e) WACCM Sulfur Injection - RCP8.5
End of century

Figure 6. Same as Figure 5, but for Sulfur Injection using WACCM. The first row: P/PET in the bias-corrected output of the model at the present day (unitless). The second row: (b) The projected baseline changes at the mid-century (%) relative to present-day; (c) The mitigation of the baseline changes, relative to present-day. The third row: same as the second but for the end of the century. The similar P/PET changes in absolute values (unitless) can be found in row 1 of Figure 2.

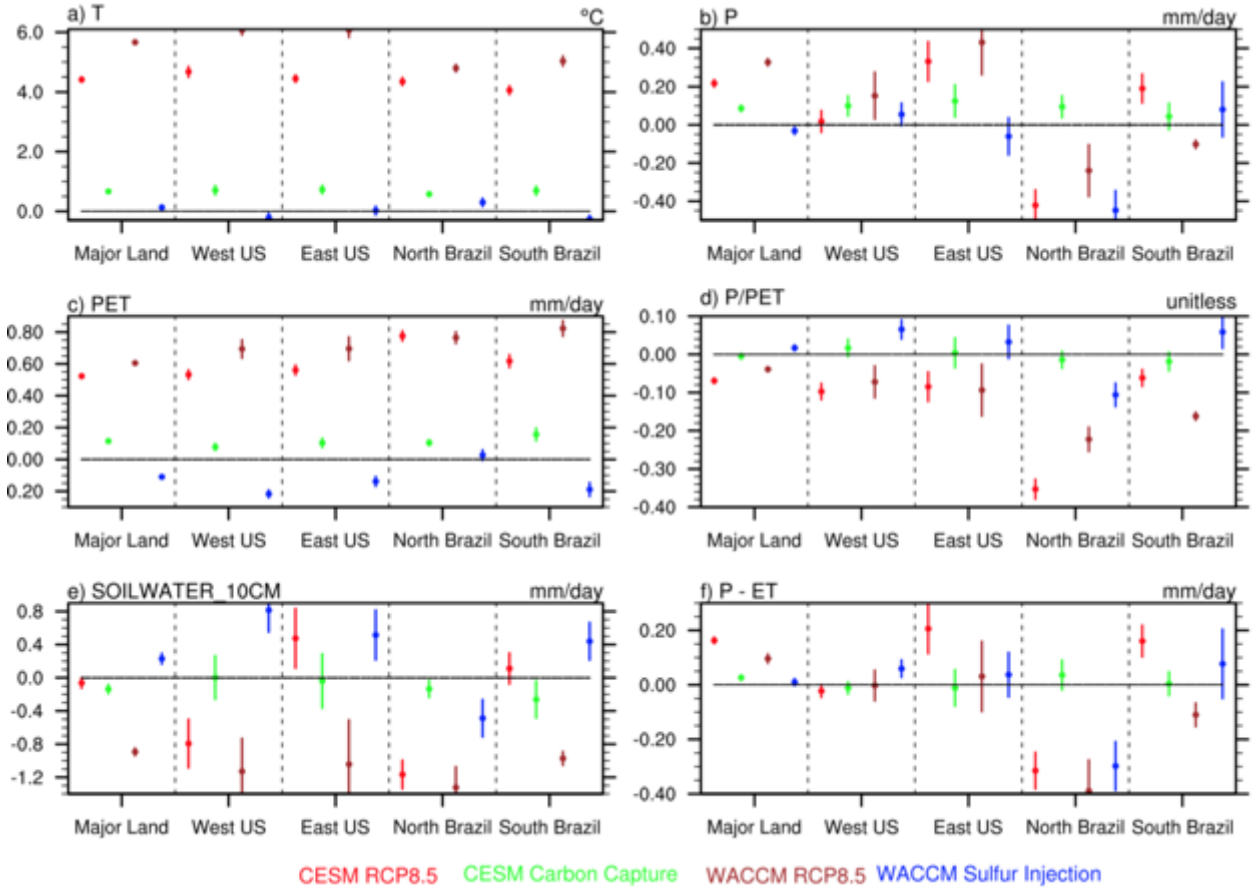

Figure 7. Regional changes at the end of the century relative to the present-day. Western and Eastern US are separated by 100ºW, and Northern and Southern Brazil are separated by 10ºS. See the boxes in Figure 5a for the domains. The zero lines of the y-axis indicate the present-day level.

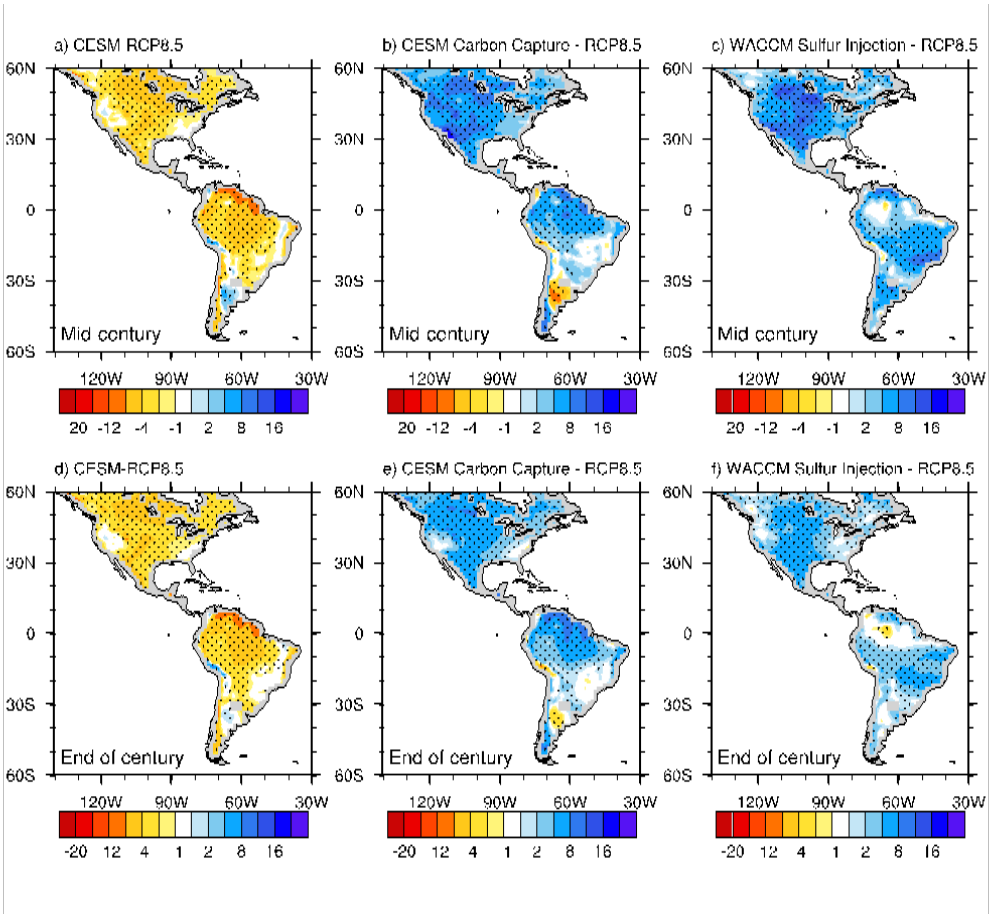

Figure 8. Similar to Figure 5's 2nd and 3rd rows but showing normalized P/PET change in %/ºC. (a)-(c) are mid-century changes, and (d)-(f) are end of century changes. The normalization is by scaling the global temperature change in the right two columns, for example, 4.2ºC due to Carbon Capture in panel e and 6.0ºC due to Sulfur Injection in panel f.

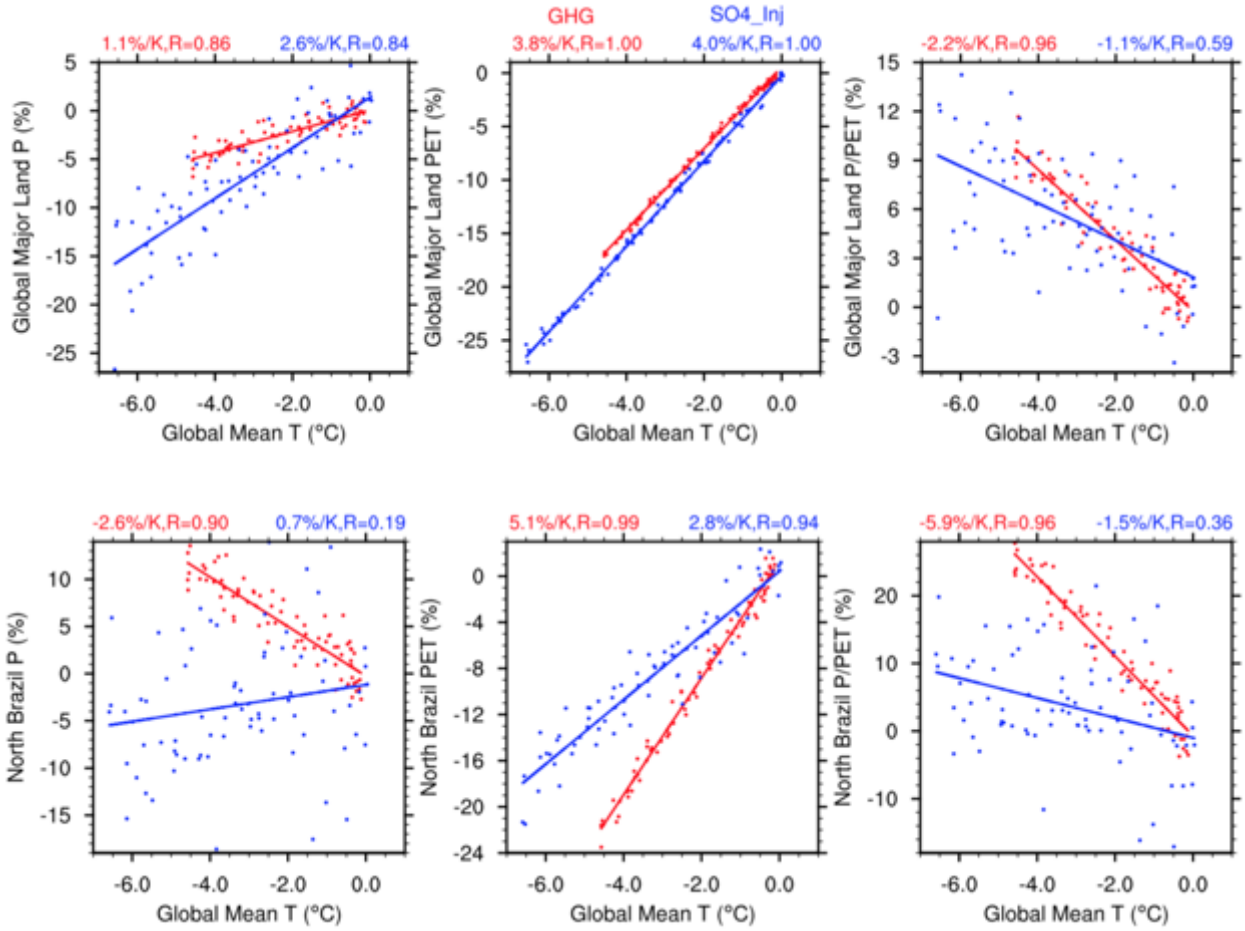

Figure 9. The changes of global major land P, PET, and P/PET as a function of global mean temperature change (ocean+land). Each dot represents a model year during 2020-2097. Red is for Carbon Capture (using CESM), and blue is for Sulfur Injection (using WACCM). (top) global land; (bottom) North Brazil.

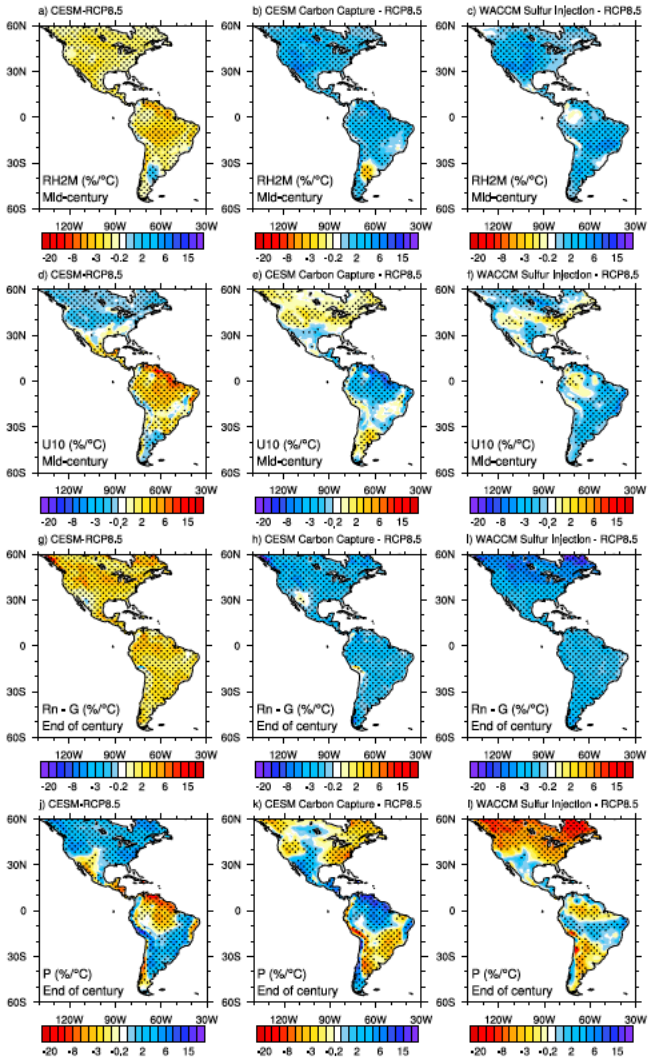

Figure 10. Similar to Figure 8 but showing (Row 1) RH2M (relative humidity, normalized change in %/ºC). (Row 2) U10 (surface wind, normalized change in %/ºC). (Row 3) Rn-G (surface available energy, normalized change in %/ºC). (Row 4) P (precipitation, normalized change in %/ºC). Left panels show the changes in baseline warming. Middle panels show mitigated change due to carbon capture. Right panels show the mitigated change due to sulfur injection. Note that, for simplicity, we only show RH2M and U10 results for mid-century, and Rn-G and P results for the end of the century.